Chapter 4

Episodic dissolution, precipitation and slip along the Heart Mountain detachment, Wyoming

Erika M. Swanson[1], Brian P. Wernicke[1], and Thomas A. Hauge[2]

1: Division of Geological and Planetary Sciences

California Institute of Technology

Pasadena, CA 91125

2: 3519 S. Main St.,

Seattle, WA 98144

In preparation for submission to Tectonics

ABSTRACT

The Heart Mountain allochthon is among the largest landslide masses in the rock record. The basal fault, the Heart Mountain detachment, is an archetype for the mechanical enigma of brittle fracture and subsequent frictional slip on low-angle faults, both of which appear to occur at ratios of shear stress to normal stress far below those predicted by laboratory experiments. The location of the detachment near the base of thick cratonic carbonates, rather than within subjacent shales, is particularly enigmatic for frictional slip. A broad array of potential mechanisms for failure on this rootless fault have been proposed, the majority of which invoke single-event, catastrophic emplacement of the allochthon. Here, we present field, petrographic and geochemical evidence for multiple slip events, including cross-cutting clastic dikes and multiple brecciation and veining events. Cataclasites along the fault show abundant evidence of pressure solution creep. "Banded grains," which have been cited as evidence for catastrophic emplacement, are associated with stylolitic surfaces and alteration textures that suggest formation through the relatively slow processes of dissolution and chemical alteration rather than suspension in a fluid. Temperatures of formation of fault-related rocks, as revealed by clumped isotope thermometry, are low and incompatible with models of catastrophic emplacement.

We propose that displacement along the detachment was initiated near the base of the carbonates as localized patches of viscous yielding, engendered by pressure solution. This yielding, which occurred at very low ratios of shear stress to normal stress, induced local subhorizontal tractions along the base of the allochthon, raising shear stress levels (i.e., locally rotating the stress field) to the point where brittle failure and subsequent slip occurred along the detachment. Iteration of this process over many years produced the observed multi-kilometer displacements. This concept does not require conditions and materials that are commonly invoked to resolve the "stress paradox" for low-angle faults, such as near-lithostatic fluid pressures or relative weakness of phyllosilicates in the brittle regime. Cyclic interaction of pressure solution

creep and brittle failure may occur under any fluid pressure conditions and within any rock type, and as such may be an attractive mechanism for slip on "misoriented" fault planes in general.

INTRODUCTION

Fracture and slip on shallowly dipping detachments is one of the longest-debated puzzles in tectonics. According to the classic Andersonian theory of fault mechanics, which assumes coulombic failure criteria with one vertical principal stress axis, the ratio of shear stress to normal stress is far too low for both initiation and continued slip on normal faults dipping less than 30 degrees (e.g. Axen, 2004). Even under the ambient condition of lithostatic pore fluid pressure, slip along low angle planes is not predicted to occur before more favorably oriented slip planes are all well above their failure criteria (e.g. Collettini, 2011). However, many geologists have documented that the dominant structures in the upper crust in extensional environments are often shallowly dipping detachments (e.g. Armstrong, 1972; Davis and Coney, 1979; Pierce, 1980; Allmendinger et al., 1983; Wernicke et al. 1985; Hauge, 1985, 1990; Lister and Davis, 1989; Wernicke, 1995; Morley, 2014).

The Eocene Heart Mountain detachment in northwestern Wyoming is among the largest, best-studied examples of such an enigmatic feature (Figure 1). Extant exposures of the upper plate of the detachment, the Heart Mountain allochthon, form an elongate, internally coherent, extended mass comprising Paleozoic carbonate strata and overlying Eocene Absaroka volcanics. The allochthon is at least 70 km long, with apparent slip of as much as 45 kilometers (e.g. Pierce, 1980). At present, the base of the allochthon is subhorizontal (<10° dip), and exposed within a narrow range of elevation (c. 1800 – 2800 m). A contour map of the fault surface defines a gently warped, dome-and-basin structure, with little or no systematic slope over its area of exposure (Figure 2).

Since its discovery in the late 19th century, varied aspects of the origin and emplacement history of the Heart Mountain allochthon have been hotly debated. A conspicuous klippe of Paleozoic carbonates over Eocene sedimentary units in the basin at Heart Mountain (Figure 1) was first recognized by Eldridge (1894) and described again by Fisher (1906). Further study revealed more apparent klippen to the west with similar structural characteristics, leading Dake (1918) to suggest emplacement by thrust faulting. The observation that hanging wall structure primarily reflects horizontal extension (Bucher, 1947) suggested that the allochthon, comprising Paleozoic blocks, was emplaced rapidly as discontinuous, "individual fragments," perhaps in response to seismic activity antecedent to volcanism.

The detachment zone and environs were first systematically mapped at relatively small scale by a US Geological Survey team led by W. G. Pierce (Pierce, 1965a, 1965b, 1966, 1978; Pierce and Nelson, 1968, 1969, 1971; Pierce et al, 1973, 1982; Prostka et al, 1975). These workers also concluded the allochthon was emplaced *just prior* to most local Absaroka volcanism, leaving much of the original detachment surface subaerially exposed, effectively as a large-scale landslide scar (Pierce, 1957; 1973). According to this "tectonic denudation" hypothesis, before significant erosion had occurred, the exposed surface was unconformably overlain by a thick sequence of *post*-emplacement volcanic strata.

Kinematics: Catastrophic versus Gradual Emplacement

The "denudation hypothesis" raised two fundamental questions about the kinematics of displacement that must be addressed before any serious attempt can be made towards understanding the mechanics of slip along the detachment. The first is whether the allochthon was a contiguous mass during emplacement, or fragmented into isolated blocks. The second is whether or not emplacement was catastrophic (occurring in a few minutes or hours), or gradual, perhaps occurring on a million-year timescale.

In regard to the first question, a detailed, systematic structural analysis of the best-exposed traces of the contact between the putatively post-emplacement volcanics and the footwall of the detachment suggested that volcanic rocks in contact with the footwall are generally tilted and faulted against it, not extruded onto it (Hauge, 1982). These observations led to the hypothesis that the hanging wall of the detachment, on the eastern flank of the extensive Absaroka Volcanic Field, deformed as a continuous, extending allochthon above a detachment plane that remained in the subsurface throughout its movement history, rather than being denuded and, briefly, subaerially exposed prior to magmatism (Hauge, 1985).

In regard to the second question, Hauge (1985, 1990) and Beutner and Hauge (2009) proposed that the allochthon was emplaced, at least in part, gradually rather than catastrophically. They cited structural features in the allochthon such as calcite growth fibers along faults, mesoscale superposition relations among diking and faulting that require more than one event, and multiple brecciation events, which indicate at least some progressive deformation, rather than a single catastrophic event. Further, biotite Ar-Ar plateau ages determined on a trachytic ash-flow tuff (50.01 ± 0.14 Ma) that overlaps the “breakaway” fault in its northeasternmost area of exposure (Figure 1) are significantly older than the age of a monzogabbro intrusion (48.21 ± 0.08 Ma; Hiza, 2000) that is cut by the fault in its central area of exposure at White Mountain (Figure 1), suggesting that the allochthon was active over a period of nearly 2 Ma.

At present, there is thus apparent consensus that (1) the allochthon is a continuous, extended mass in which (2) large volumes of volcanics are involved in faulting; and given its extant area of exposure of over 2,100 km^2, (3) it constitutes perhaps the largest known subaerial landslide in the geological record (Beutner and Gerbi, 2005; Beutner and Hauge, 2009; Goren et al., 2010; Craddock et al., 2012; Anders et al., 2013). However, opinion remains sharply divided on the kinematic question of the whether emplacement was catastrophic (Anders et al., 2010; Craddock et al., 2012; Goren et al., 2010) or, at least in part, gradual (Hauge, 1985, 1990; Beutner and Hauge, 2009), limiting progress toward understanding the dynamics of slip.

Dynamics: the Stress Paradox

The debate about the mechanics of slip has traditionally been influenced by two longstanding issues related to stresses that drive low-angle faulting, (1) their unfavorable orientation in the context of Andersonian mechanics (e.g. Colletini and Sibson, 2011), and (2) the potential role of pore fluid pressure acting on an impermeable allochthon, in resolving the paradox (Hubbert and Rubey, 1959; Rubey and Hubbert, 1959). In the case of Heart Mountain, the dip during initiation and slip is very low (Figure 2), making the stress ratio problem particularly acute. In addition, the allochthon is thin (c. 1-2 km, aspect ratio c. 50:1; Figure 1b) and its base includes highly fractured, presumably highly permeable carbonates, making both the development and maintenance of elevated fluid pressure problematic (Davis, 1965).

Given these facts, any mechanical conception of the Heart Mountain detachment as forming catastrophically has at its disposal a broad palette of extraordinary circumstances, affecting and area of thousands of square kilometers (e.g., fluid overpressure, magmatic devolatilization, seismic accelerations, bolide impact, etc.) that only need to operate for as little as a few seconds prior to emplacement, rather than a million years or more (e.g. Hughes, 1970; Pierce, 1973, 1980; Voight, 1973; Sales, 1983; Melosh, 1983; Beutner and Gerbi, 2005; Aharonov and Anders, 2006; Craddock et al., 2009, 2012; Anders et al., 2010, 2013). The gradual emplacement hypothesis, on the other hand, restricts the system to processes that either function continuously, or at least are repeatable thousands of times, on a million-year time scale (e.g. Hauge, 1982, 1985, 1990, 1993a; Templeton et al., 1995; Hiza, 2000; Douglas et al, 2003; Beutner and Hauge, 2009). As such, the gradual emplacement model, if correct, starkly exposes traditional conceptions of brittle fault mechanics as having little explanatory power.

The implicit assumption that fault displacement in the upper crust is controlled entirely by brittle fracture and frictional sliding criteria has come under question. It is clear from the rock record that significant strains in the brittle regime are absorbed by pressure solution (e.g.

Engelder 1979; Wright and Platt, 1982), and is likely an important factor along brittle faults (e.g. Collettini and Holdsworth, 2004; Anderson et al., 2010). In contrast to other known low- to moderate-temperature deformation processes, both theoretical arguments and experimental data suggest that pressure solution in rocks and minerals has a viscous rheology (e.g. Rutter, 1983; Bos and Spiers, 2004). Gratier et al. (2002, 2013) have described how pressure solution creep and crack sealing may exert significant control over the seismic cycle and mechanics of strike-slip faults. If pressure solution creep played a significant role in Heart Mountain faulting, the mechanics of low-angle faulting in general may benefit from re-evaluation.

With the issues of catastrophic versus gradual emplacement, and the potential role of fluid-assisted deformation in mind, we conducted a detailed mesoscopic and microscopic analysis of structural features on and near the Heart Mountain detachment in key localities, in coordination with a sampling program to study the temperature and isotopic composition of fluids associated with faulting using carbonate clumped-isotope thermometry. Here we report the results of our analysis of mesoscopic and microscopic structural features, as well as clumped isotope data pertinent to their interpretation. In a companion paper, we present the bulk of our isotopic results that bear on the origin and evolution of fluids along fault (Swanson et al., submitted).

HEART MOUNTAIN DETACHMENT AND EXTENSIONAL ALLOCHTHON

At large scale, the Heart Mountain detachment is divisible into three main areas based on the footwall detachment level, which from northwest to southeast includes the “Paleozoic,” “ramp” and “Eocene” footwall sections (Pierce, 1980; Figure 1). The detachment initiated predominantly as a decollement within the Paleozoic sections, ramping steeply upward across Paleozoic and Mesozoic strata, and then cutting gently upsection to the SE within Eocene strata.

The hanging wall, or “extensional allochthon,” roughly doubled in areal extent as a result of internal extension, bringing Eocene volcanic rocks down into direct contact with the Paleozoic section, and translating Paleozoic strata in the hanging wall over Eocene sediments of the Bighorn basin.

The carbonate component of the allochthon is a cratonic Paleozoic section approximately 500 m thick, ranging from Ordovician to Mississippian in age. The overlying volcanic component includes Eocene volcanic strata of the Absaroka Volcanic Supergroup (c. 52-48 Ma) and related dikes and small intrusive bodies. The basal decollement initiated within a remarkably narrow stratigraphic interval (<5 m) near the base of the Ordovician Bighorn Dolostone (e.g., Pierce, 1973). Because of internal distension of the allochthon, both Paleozoic and overlying Tertiary components of the allochthon are juxtaposed with the footwall (e.g. Hauge , 1985, 1990).

The fault lies along the eastern margin of the extensive Absaroka volcanic field, and was active during Absaroka magmatism (e.g. Hiza, 2000; Feeley and Cosca, 2003; Douglas et al., 2003). Above the Paleozoic footwall section of the detachment, the allochthon is largely co-spatial with the Sunlight Volcano, one of the easternmost elements of the field (Figure 1). The principal components of the volcano include c. 1500 m of intermediate to mafic flows of the Wapiti Formation (c. 49-50 Ma) and overlying Trout Peak Trachyandesite (c. 48.5-48.1 Ma; Feeley and Cosca, 2003), along with a well developed radial dike swarm and scattered small plutons. Because of these temporal and spatial relations, the elongate allochthon is generally regarded as a ‘sector collapse,’ generally southeastward toward the Laramide Bighorn Basin (e.g., Beutner and Hauge, 2009; Anders et al., 2010).

The detachment forms a remarkably flat, planar structure that is readily identifiable in the field, even from distances of a kilometer or more (Figure 3, a and b). Below the detachment in the Paleozoic footwall, bedding within the Ordovician Bighorn Dolostone and Cambrian Snowy Range Formation is usually subhorizontal (dips <10°), structurally intact and parallel to the detachment. In some places, the footwall is virtually undeformed below the detachment, maintaining its original form to within a millimeter or less of the fault (e.g., Anders et al., 2010). In others, significant deformation has affected the footwall below the fault (see discussion below).

In contrast to the footwall, the allochthon is pervasively faulted at kilometer scale, with hanging wall strata of both Paleozoic and Tertiary age commonly tilted to moderate dips of 20-50° (Hauge, 1985, his Fig. 2). Hanging wall faults are often associated with veins filled with sparry calcite, ranging from millimeter- to centimeter-scale in width. These veins in places exhibit calcite growth fibers, inferred to represent evidence for gradual displacement (e.g. Hauge, 1993b). Adjacent to the detachment, the allochthon is typically cut by numerous mesoscale, slickensided faults, and shattered into jigsaw breccia, autobreccia and fault gouge (Hauge, 1985). Brecciation occurs at a distance of up to tens of meters above the fault plane. In some places a tabular, texturally distinct layer ('basal layer' of Anders et al., 2010) occurs directly on the fault plane, usually ca. 1 mm thick but in one notable locality (White Mountain, Figure 1) is about 3 m thick. In most places along the fault, clastic dikes filled with fine-grained breccia and gouge are injected into the hanging wall. They occur most commonly within c. 100 m vertically above of the detachment plane (Pierce, 1979; Hauge, 1985). They range from c. 1 cm up to 1 m in width, and exhibit diverse orientations relative to the detachment. Boundaries of the dikes may be either planar and parallel to one another, or highly irregular.

OBSERVATIONS

We visited 11 sites along the exposed trace of the Heart Mountain detachment, making mesoscopic observations of field relations, and collecting 80 carbonate samples for analysis, including fault rocks, clastic dikes, veins and Paleozoic host rocks, spanning a NW-SE distance of 70 kilometers, from near the “breakaway” in the northern part of the allochthon to its “toe” in the Bighorn Basin at Heart Mountain (Figure 1). Including some 80 thin sections archived from an earlier study (Hauge, 1983) we analyzed a total of 117 thin sections using a petrographic microscope. To verify petrographically based mineral identifications, a subset of 8 samples were analyzed by SEM imaging and EDS. We performed a total of 83 carbonate clumped-isotope analyses from our sample suite, six of which are presented here because of their relevance to superposition relationships along the detachment zone, with the remainder presented in Swanson et al. (2015). A brief description of analytical methods for clumped isotope thermometry is presented in Appendix A.

Mesostructural Observations

We observed cataclasis in the footwall, from thin section scale up to several meters below the detachment. Localities where we observed footwall cataclasis include, from north to south, Silver Gate, Colter Pass, Jim Smith Creek, Pilot Creek, Cathedral Cliffs, and Hoodoo Creek, respectively. Among the best developed of these zone is at Jim Smith Creek. There, the upper 2 to 3 m of Bighorn Formation below the detachment developed a structural fabric through intense brecciation and fluid alteration, which is truncated by the detachment (Figure 3, a and c).

There is also macroscopic evidence of polyphase brittle deformation, where older fault-related features are offset or folded by younger ones. For example, at Fox Creek, Heart Mountain, and Crandall Creek (Figure 3, d, e and f, respectively), earlier gouge zones or clastic dikes are overprinted by faulting, flexure and brecciation in association with mesoscale faults.

At Fox Creek, about 5 to 10 meters above the detachment, multiple episodes of injection of clastic dikes are observed, with both cross-cutting dikes and “sheeting” or multiphase injection apparent within the same dike (Figure 4). There, the widest dike is about 10 cm thick, with a darker colored, older injection phase preserved along the margins overprinted by a lighter colored, younger phase (Figure 4, a and b). The lighter colored core phase has a lower percentage of coarse clasts than the darker phase on the margin. The lighter core phase of the main dike is physically contiguous with a thinner dike that projects into the country rock, where it sharply truncates two older dikes at right angle, one of which is a darker, fine-grained phase and the other a lighter, coarse grained phase (Figure 4c). Both relationships suggest at least two episodes of injection. In addition, the host rock itself is strongly brecciated Bighorn Formation, requiring a third, older event to cause the brecciation. Within a few meters of the two-toned clastic dike, there are three smaller dikes that form an en echelon pattern, each about 20 cm long and with an apparent dip of ~30° towards the south (Figure 4d). Assuming the clastic dikes are tensile features and have not been tilted, they imply that the principal stress orientations at the time of injection were not vertical, but rather favorable for top-south shear (Figure 4d). Additional deformation events are recorded by mesoscale fault offsets of the main clastic dike. The margin and darker, exterior phase are offset by two different faults, but the lighter, interior light-colored phase is only offset by one of the faults (Figure 5), suggesting that mesoscale faulting was active during dike injection.

In sum, given that both diking and faulting overprint brecciated country rock, we interpret there to have been at least five discrete deformational events at Fox Creek, including (1) brecciation of host Bighorn Formation, (2) injection of dark-colored phase of main clastic dike, (3) offset of the dike by about 4 cm (left-hand fault of Figure 5), (4) injection of the light-colored phase of the clastic dike, and (5), offset of the dike by about 4 cm (right-hand fracture in Figure 5). The brecciation and diking events must have been separated by sufficient time to lithify the material, which we presume was cohesionless at the time of formation.

Microstructural Observations

Breccia clasts within breccias

Evidence for breccia clasts that are themselves breccias is ubiquitous, and occurs in both the hanging wall and footwall of the detachment (Figure 6). In some cases, breccia clasts contain boundaries between clasts of volcanic fragments in a matrix of carbonate breccia (Figure 6a). In others, we observe vein systems that, although they may mainly postdate brecciation, exhibit textures suggestive of progressive deformation after brecciation had ceased (Figure 6b). In the footwall of the detachment at Jim Smith Creek, re-brecciation (Figure 6c) included examples that record the generation of three different textures of breccia (Figure 6d). Veining at this locality appears to be syntectonic with brecciation. In addition to White Mountain, Squaw Creek and Jim Smith Creek, multiple episodes of brecciation are recorded in samples from Silver Gate, Falls Creek, Colter Pass, Fox Creek, Cathedral Cliffs, Crandall Creek, and Heart Mountain.

Some clasts contain veins that cross-cut an older brecciation event, and are in turn truncated by a younger one (Figure 6, e and f). The formation of these textures record, at a minimum, the following sequence of events: (1) brecciation of the host rock, (2) lithification of the granular material, (3) fracture and progressive precipitation of vein fill; (4) a second brecciation event, followed by (5) final lithification. Further repetitions of steps 1 and 2 are indicated for clasts with more than two brecciation events, as in Figure 6d. Because each brecciation event reduces the average grain size of previous events, it would seem unlikely that any given sample would have the capacity to record more than a few events, regardless of the total number events accommodated by the fault. The observed textures, in other words, may well be "saturated" in terms of their ability to record a much larger number of events than those observed.

Banded grains

Heart Mountain detachment breccias, particularly at White Mountain, contain rounded grains with concentric color-banding, shown in Figure 7. Except at White Mountain, these grains tend to be scarce. First noted by Hughes (1970), they have variously been referred to as "accreted grains," "armored grains" or "mantled grains" by Beutner and Craven (1996, their Figure 4), Beutner and Gerbi (2005, their Figures 6 and 7), Craddock et al, 2012 (their Figure 3), Anders et al., 2010 (their Figures 3d and 4), and Craddock et al 2009 (their Figure 3e). We prefer instead the nomenclature "banded grain" as a non-genetic, wholly descriptive, term because it does not presuppose that the banding represents augmentation of a pre-existing grain, as implied by the genetic terms "mantled," "armored" and "accreted."

These grains show considerable diversity in their appearance, but all consist of a core grain surrounded by a dark-colored band. There is no apparent pattern in regard to the size or composition of the banded grains versus "normal" grains. Electron probe microanalysis shows that major cation ratios are not affected by the color banding, indicating that it originates from submicron-scale trace mineralization. However, in some instances, both inside and outside the exterior dark band, the matrix exhibits concentric flattening, with long axes oriented tangentially to the core. Beyond these similarities, the grains may be subdivided into two main types, which we will refer to informally herein as "Type 1" and "Type 2."

In Type 1 grains, a rigid core differs little from the matrix, and there is a single band of dark material that surrounds it. Outside the dark band, the matrix sometimes exhibits inhomogeneous, concentric flattening, forming an diffuse, exterior "halo" up to several grain radii outward from the dark band (Figure 7a through d; Figure 8b). In one instance, we observed a strongly flattened, Type 1 banded grain within the halo, implying the formation of these grains is a protracted process (Figure 7b).

In Type 2 grains (Figure 7e through h), the core is smaller than the outer dark band, and the intervening part of the grain forms a light-colored ring or "bleached halo," inside the grain, usually with diffuse inner and outer margins. In some examples, multiple fine-scale banding is observed within or around the margins of the grains (Figure 7f). In one example, the color pattern is reversed, with the interior halo forming a darker band than the core and outer ring. However, in general the darkest layer in the banding is at the outer edge of the grain.

The cores are diverse in composition for both grain types, and include (1) volcanic phenocrysts, (1) authigenic minerals. (2) volcanic rocks and their alteration products (clays, yellow-hued (zeolite?) grains), (3) carbonate rock, and (4) breccia, that may include both carbonate and volcanic grains. The alteration bands of both the outer dark rings and the interior, bleached halos cuts across older textures (Figure 7, e and f). In Figure 8a, the light brown zone of alteration surrounding a core grain overprints an older dark brown layer, which in turn truncates breccia from an earlier event.

Further observations pertinent to progressive development include evidence that pressure solution may be associated with the formation of banded grains, as shown in Figure 8b. In this sample, a (previously) rounded carbonate grain is truncated by the dissolution seam around the edge of the banded grain. Surrounding grains in the ~100 μm range exhibit tangential flattening parallel to the edge of the core grain. The flattening may also reflect increased pressure solution tangential to the grain.

A few grains show rims similar to those in banded grains, but which are generally smaller and of highly variable thickness around the core grain (Figure 8, c and d). The contact between the dark brown rim material and the host grain is often irregular, with concavities that we interpret to reflect alteration of the host into the rim material. A similar dark band surrounds non-spherical grains, including ones with a high aspect ratio (e.g. Figure 8e). These dark seams have a similar color and texture to stylolites, but are round.

The frequency of occurrence of banded grains varies, but never surpasses 10% of the area of any given thin section, with the remainder of the rock having a "normal" cataclastic texture. The highest percentage of banded grains (up to 10%) is observed at White Mountain. Banded grains were common but weakly developed within a hanging wall fault at Heart Mountain, where they comprised up to 5% of the rock. A few other localities showed banded grains, but very infrequently, and with poorly defined banding. These localities include clastic dikes with a large fraction of volcanics, such as that found at Crandall Creek and Jim Smith Creek. The majority of samples we collected did not show any evidence of concentrically banded grains.

Pressure solution creep

In the majority of samples collected, there is abundant evidence for pressure solution. Evidence includes truncation and interpenetration of contrasting textural phases (Figure 9, a through f), accumulation of iron oxide and insoluble residues (Figure 9 a, b, and d), the lack of through-going localized slip surfaces (Figure 9, c, e, and f), and ductile deformation fabrics, despite shallow crustal depths (<2000 m) of deformation (Figures 10 and 11).

A sample from Pilot Creek (Figure 9d) shows a number of pressure solution seams cross-cutting an older breccia, which are truncated by a younger brecciation event. The cross-cutting relationships require that the pressure solution features were created after the first brecciation but before the second brecciation, with enough time between to dissolve the carbonate along the seams.

A sample from Jim Smith Creek shows a hanging wall comprised of volcanic breccia overlying a footwall of carbonate breccia, separated by a 2-mm gouge zone along the detachment surface (Figure 10). A clastic dike within the hanging wall is visibly connected to, and texturally identical to, the gouge. The volcanic hanging wall includes both carbonate xenoliths and hornblende phenocrysts deformed into sigmoidal shapes in a shear zone within a few centimeters of the detachment plane (Figure 10). This fabric is similar to those commonly observed in mid-crustal tectonites dominated by dislocation creep, but its structural position within Absaroka volcanic units precludes a depth of more than 1.5 km. Further, the shear zone was syn-tectonic with injection of clastic dikes originating in a thin basal layer of breccia. The shear zone truncates the clastic dike, and is in turn truncated by the detachment. As described below, the sigmoidal shapes of the grains within the shear zone are likely to be a textural manifestation of pressure solution along the shear zone, rather than dislocation creep, which in any event is unlikely. These cross-cutting relationships indicate that pressure solution creep occurred at the same time as slip on the detachment.

Clumped Isotope Thermometry

We measured the carbon, oxygen, and clumped-isotope compositions of a six-sample transect of samples across the color boundary of the two-toned clastic dike exposed at Fox Creek (Figure 4e, Table 1). These results indicate that the outer, dark material (samples A, B, and C) is 13° C warmer than inner, light material (samples D, E, and F). Despite the temperature difference, the samples have indistinguishable bulk carbon and oxygen isotope composition. Texturally, these samples are mixtures of material, and the difference in observed temperatures can either result from different ratios of the same cold and warm material formed prior to diking, or they can result from different crystallization temperatures of material during injection. Either way, the injections of cataclasite responsible for the two-toned pattern were two discrete events.

The recorded temperatures are relatively cold for fault-related samples (see Swanson et al., 2012; Swanson et al., submitted), and much colder than that expected for a rapidly slipping fault zone at the base of a collapsing, active volcano. The inner clastic dike samples are colder than the host Bighorn Formation, while the bulk carbon and oxygen isotopes of the mineral are consistent with the host rock. The $\delta^{18}O$ of the waters in equilibrium with the samples are near the lower limit of the host rock range for the light-colored, inner clastic dike material. This requires recrystallization of at least some of the carbonate under cold conditions, and likely results from precipitation of small amounts of carbonate while at the cold surface, and exposed to meteoric water. These data do not show any signs of recrystallization under high temperature conditions, as might be expected from frictional heating or injection of volcanic gases along a fault.

DISCUSSION

Brecciation and veining events

Both mesoscopic and microscopic evidence described above, as well as similar observations by Hauge (1985, 1990), provide abundant evidence for multicyclic fragmentation, clastic diking, and pressure solution events along the detachment plane, casting serious doubt on the hypothesis that emplacement of the entire allochthon was a single, catastrophic event. As we discuss below, we suspect that not only was emplacement not catastrophic, but that the key evidence previously used in favor of it may instead be interpreted as evidence in favor of gradual emplacement by a combination of cataclastic flow (pressure-sensitive rheology) and viscous flow (rate-sensitive rheology), over a protracted period of time.

Evidence for multiple slip events, in the form of clasts of breccia within younger breccia, was presented previously, including by researchers who interpret the slip along the Heart Mountain detachment to be catastrophic (see Anders et al., 2010, their Figure 4e; Craddock et al., 2009 , their Figure 3; Beutner and Gerbi 2005, their Figures 6 and 7; Beutner and Craven 1996, their Figure 4). However, these authors all dismiss this brecciation as either deformation that occurred earlier in the catastrophic event (Anders et al, 2000), or “pre–Heart Mountain detachment deformation” (Craddock et al 2009). They do not explain their reasons for interpreting the deformation that was observed only along the Heart Mountain detachment as being unrelated to slip along that fault. We believe the more likely explanation for multiple phases of brecciation along the fault is that multiple slip events occurred along the fault.

In addition to multiple brecciation events, there is evidence for multiple veining events, as shown in Figure 6b. The change in orientation of the calcite crystals indicates deformation during growth. A later, more iron-rich fluid resulted in crystallization of the en-echelon structure in Figure 6b.

Banded Grains

Previous studies discussing the presence of banded grains similar to those in Figures 7 and 8, interpret them as having formed during suspension within a pressurized fluid at the base of the detachment, and constitute evidence of catastrophic slip (Hughes, 1970; Beutner and Craven, 1996; Beutner and Gerbi, 2005; Craddock et al., 2009 and 2012; Anders et al., 2010).

In the discussion of the processes that might have created the banded grains, the analogues of volcanic accretionary lapilli and impact ejecta were invoked, with an interpreted fluid of volcanic gas preferred for Heart Mountain (e.g. Beutner and Gerbi, 2005). However, in these analogues, the clasts with accretionary rims make up a very high percentage of the rock, at least 90% (see Beutner and Gerbi, 2005, their figures 8, 9, and 10), and the remaining 10% of material is the matrix, not uncoated grains. Later authors adopted the same mechanism of suspension in a fluid to explain the presence of “accreted grains”, albeit with an interpreted CO_2 fluid, formed from massive decomposition of carbonate during frictional heating (e.g. Anders et al., 2010). If the same accretionary processes are present along the Heart Mountain detachment, a similarly large proportion of accreted grains might be expected, but is not observed. Additionally, one might expect that suspension would affect grains according to size, with the smaller grains, which are more likely to be suspended, preferentially showing coatings. There is no apparent correlation between the size of the grains that have rims compared with those that do not in the examples in Figures 7 and 8.

We prefer the interpretation that these grains formed by alteration and dissolution processes rather than accretionary processes. Close inspection of the surfaces bounding many of the banded grains shows a remarkable similarity in texture, color, and general appearance to stylolites. Only the overall round form appears to distinguish them from “normal” stylolites. The process that could produce spherical or ellipsoidal pattern of dissolution is not entirely clear, but it is not unprecedented (Figure 8 f). A sample from a low-angle detachment within carbonate in the Mormon Mountains in Nevada shows an example of a continuous stylolite with ellipsoidal regions. Perhaps this represents an early stage of formation of the banded grains.

It is possible that the formation of banded grains is similar to the production of corestones, like those in weathered granite. In corestone formation, the material within the corestone is compositionally exactly the same as the surrounding material, but experienced less weathering. These banded grains might be similar, in that they are simply regions that experienced less dissolution that the surrounding rock. This explanation is speculative, but its strengths include explanation for (1) the low percentage of concentrically banded grains, (2) the lack of correlation between grain size and putative accretion, (3) the variability of compositions of the grain cores, and, perhaps most importantly, (4) the truncation of matrix grains by the banding (e.g. Figure 8b). This possibility was acknowledged by Beutner and Gerbi (1996), but not preferred due to a lack of insoluble residues and their observations that “small carbonate grains in contact with films show no evidence of grain shaping by dissolution.” Our petrographic observations show both of these types of features are present (Figures 7 and 8b).

Banded grains, also referred to as “clast-cortex grains,” have been described in rooted faults, including the carbonate-hosted Tre Monti fault in Italy (Smith et al., 2011). This texture was proposed to be a potential indicator of rapid slip, in part because of the similarity to “armoured carbonate grains found within the basal detachment horizons of catastrophic landslides,” with the citations referring solely to studies of the Heart Mountain basal layer (Smith et al., 2011). These authors called for experiments to constrain the possible rates of slip that can form banded grains, before applying this texture to interpretations of slip. Han and Hirose (2012) created similar concentrically banded grains (their “clay-clast aggregates”) via experiments using quartz-bentonite gouges, including at slip rates 3 orders of magnitude slower lower than seismic slip rates (0.0005 m/s). However, to our knowledge, analogous studies in carbonate rocks have not been done.

Mechanism for slip on the Heart Mountain detachment

A potential mechanism that may have facilitated slip on the apparently unfavorably oriented Heart Mountain detachment is pressure solution creep along the detachment surface that occurs in heterogeneous patches, which elastically load areas of the fault between them with additional subhorizontal shear tractions. This loading may have the effect of locally rotating the principal stress directions in the vicinity of the fault, enabling brittle failure on the detachment surface (Figure 12a). A section of fault that is not creeping (or creeping much more slowly) by pressure solution and reprecipitation is shown in the middle (with a thin black line), with sections that creep on either side (thick gray line). The section that does not creep will experience forces due to gravity, the upward normal force from the footwall, and an updip force due to friction (all black arrows), but also an additional down-dip shear traction from elastic strain (red arrows). The inclusion of elastic forces in the force diagrams results in a different state of stress than that predicted solely from gravity, and result a locally non-vertical maximum compressive stress (Figure 12b).

A maximum compressive stress that is not vertical can resolve the stress paradox. With sufficient forcing from elastic strain, surfaces at low angle to the horizontal can become the preferred brittle failure direction. Under these conditions, any slight elevation of pore fluid pressure or increase in differential stress would cause brittle failure and small-magnitude displacement along the low-angle plane, including the parts that were previously creeping. The majority of the slip along the detachment need not be accommodated by pressure solution creep for this mechanism to apply.

Supporting evidence for non-vertical principal stress directions in the vicinity of the fault may be found in Riedel shear fractures that cross-cut fine-grained breccia along the detachment at Jim Smith Creek (Figure 12 c and d), as well as the geometry of en-echelon clastic dikes mentioned earlier (Figure 4 d). These Riedel fractures either result from late-stage motion along the detachment, or are post-detachment in age. At present, the detachment breccia layer is nearly horizontal, and is cut by shear fractures that are at ~80° and ~20° to the horizontal. This corresponds to an orientation of maximum compressive stress at about 50° to the horizontal, and a minimum compressive stress at 50° (e.g. Sylvester 1988), indicating the principal stresses were inclined at the time of fracture (Figure 12 b and c).

The process of elastic loading could result from any number of deformation processes, including calcite twinning, brittle creep, or other low-temperature deformation mechanisms. It is the heterogeneity of the deformation that is responsible for the elastic loading, not the specific mechanism itself. We chose to focus on pressure solution creep due to its prevalence in the samples we observed, but do not expect it to be the only important process here or along other low-angle faults.

This cyclic pressure solution-precipitation-slip model for motion on low-angle or unfavorably oriented fault zones could explain several otherwise enigmatic observations related to the Heart Mountain detachment. In particular, given that the coulombic failure strength of shale is as much as a factor of 2-3 lower than dolomite, why did the detachment localize near the base of the Ordovician dolomite layer, just above the shales? Why did it fail to break at a higher angle? Pressure solution may provide an answer to both of these questions. Under the pressure solution deformation regime, the high permeability of dolostone may make it more prone to dissolution.

CONCLUSIONS

There is an abundance of evidence that the Heart Mountain detachment moved multiple times, with some lines of evidence requiring five or more episodes of slip. Many more than five phases of deformation are envisioned, but the process of multiple overprinting renders the preservation of many more events unlikely. Many of the detachment-related rocks exhibit fault zone textures and footwall deformation that suggest a complex history of deformation. Pressure solution features are common, must form between brittle events, and likely play a role in the cyclic deformation of the Heart Mountain detachment.

The observation most commonly used in support of a single catastrophic event and fluidization of the basal layer, the banded grains, is here re-interpreted to indicate slow deformation due to dissolution and alteration. We suggest that pressure solution creep along the base of a carbonate aquifer may alter the local stress field so that coulombic failure and subsequent brittle slip on the low-angle Heart Mountain detachment is favorable.

Appendix A. ISOTOPIC METHODS

Clumped isotope thermometry is a relatively new technique used to determine the crystallization temperature of carbonate minerals. It takes advantage of the temperature dependence of the degree to which the heavy isotopes ^{13}C and ^{18}O bond to each other (Eiler, 2007). This effect can be described as an exchange reaction with the form:

$$Ca^{13}C^{16}O_3 + Ca^{12}C^{18}O^{16}O_2 = Ca^{13}C^{18}O^{16}O_2 + Ca^{12}C^{16}O_3$$

The forward reaction causes “clumping” of the heavy isotopes. The extent to which this forward reaction is favored depends on the balance between the lower vibrational energy of the ^{13}C-^{18}O bond and the entropy of the system, as described in Schauble and others (2006). At higher temperatures, a more random distribution is favored, whereas at lower temperatures, clumping is preferred. This degree of ordering is set during crystallization at temperatures ~150 to 350 °C, depending on mineralogy and cooling rate, and readily modified by intracrystalline diffusion at higher temperatures (Eiler, 2007). The measured mass 47, which consists principally of $^{13}C^{18}O^{16}O$, but also minor quantities of $^{12}C^{18}O^{17}O$ and $^{13}C^{17}O_2$, is compared to that expected for a stochastic distribution, and the difference is denoted as Δ_{47}, in units of permil (Eiler, 2011). The raw Δ_{47} values are standardized by comparison to CO_2 gases heated to achieve a nearly stochastic distribution, and then corrected with procedure described below.

Powders were obtained by microdrilling, using a 0.5 mm drill bit, to extract 8-12 mg of carbonate from the hand specimen. The specific tracks that were analyzed can be found in Figure 4e. Using the sample preparation and analysis techniques described in Huntington and others (2009), the samples were reacted with phosphoric acid at 90 °C to produce CO_2 gas, which was then cleaned by established cryogenic and gas chromatographic methods and measured for masses 44–49 using a Finnegan 253 gas source mass spectrometer.

Measured values for Δ47 for each sample were corrected based on the week's heated gas measurements, and then converted into the absolute reference frame via a secondary transfer function. This function included 25°C water-equilibrated gases, 1000°C heated gases, and carbonate standards with known values in the absolute reference frame. Then an acid digestion fractionation value for 90°C acid bath of +.092‰ was applied. The corrected Δ_{47} values are empirically related to temperature using experimental data from natural and synthetic calcites, aragonites and dolomites (Bonifacie and others, in preparation).

All stated carbon isotopic ratios are $\delta^{13}C$ with respect to Vienna Pee Dee Belemnite

(VPDB), and oxygen isotopic ratios are $\delta^{18}O$ with respect to Vienna Standard Mean Ocean Water (VSMOW). Fractionation factors used to calculate the $\delta^{18}O$ composition of pore waters are from O'Neil and others (1969) and Vasconcelos (2005). Acid digestion fractionation factors were taken from Guo and others (2009) and Rosenbaum and Sheppard (1986). As all the samples discussed here are calcite-dolomite mixtures, all calculations were done for both end members of pure calcite and pure dolomite, and the $\delta^{18}O$ carbonate and $\delta^{18}O$ water values reflect a weighted average based on estimates of the calcite/dolomite ratios.

REFERENCES CITED

Aharonov, E., and Anders, M. H., 2006, Hot water: A solution to the Heart Mountain detachment problem?: Geology, v. 34, no. 3, p. 165.

Allmendinger, R. W., Sharp, J. W., Von Tish, D., Serpa, L., Kaufman, S., Oliver, J., and Smith, R. B., 1983, Cenozoic and Mesozoic structure of the eastern Basin and Range Province, Utah, from COCORP seismic reflection data: Geology, v. 11, p. 532-536.

Anders, M. H., Aharonov, E., and Walsh, J. J., 2000, Stratified granular media beneath large slide blocks; Implications for mode of emplacement: Geology, v. 28, p. 971–974.

Anders, M. H., Fouke, B. W., Zerkle, A. L., Tavarnelli, E., Alvarez, W., and Harlow, G. E., 2010, The Role of Calcining and Basal Fluidization in the Long Runout of Carbonate Slides: An Example from the Heart Mountain Slide Block, Wyoming and Montana, U.S.A: The Journal of Geology, v. 118, no. 6, p. 577-599.

Anders, M. H., Schneider, J. R., Scholz, C. H., and Losh, S., 2013, Mode I microfracturing and fluid flow in damage zones: The key to distinguishing faults from slides: Journal of Structural Geology, v. 48, p. 113-125.

Anderson, R. E., Felger, T.J., Diehl, S.F., Page, W.R., Workman, J.B., 2010, Integration of tectonic, sedimentary and geohydrologica processes leading to small-scale extension model for the Mormon mountains area north of Lake Mead, Lincoln County, Nevada, in Umhoefer, P. J., Beard, L.S., Lamb, M.A. (Eds.), ed., Miocene Tectonics of the Lake Mead Region, Central Basin and Range, Geological Society of America Special Paper 463, p. pp. 395-426.

Armstrong, R. L., 1972, Low-Angle (Denudation) Faults, Hinterland of the Sevier Orogenic Belt, Eastern Nevada and Western Utah: Geological Society of America Bulletin, v. 83, no. 6, p. 1729-1754.

Axen, G. J., 2004, Mechanics of low-angle normal faults, in Karner, G. D., Taylor, B., Driscoll, N. W., and Kohlstedt, D. L., eds., Rheology and deformation of the lithosphere at continental margins: New York, Columbia University Press, p. 46–91.

Beutner, E. C., and Craven, A. E., 1996, Volcanic fluidization and the Heart Mountain detachment, Wyoming: Geology, v. 24, no. 7, p. 595–598.

Beutner, E. C., and Gerbi, G. P., 2005, Catastrophic emplacement of the Heart Mountain block slide, Wyoming and Montana, USA: Geological Society of America Bulletin, v. 117, no. 5, p. 724.

Beutner, E. C., and Hauge, T. A., 2009, Heart Mountain and South Fork fault systems: Architecture and evolution of the collapse of an Eocene volcanic system, northwest Wyoming: Rocky Mountain Geology, v. 44, no. 2, p. 147–164.

Bos, B., and Spiers, C. J., 2001, Experimental investigation into the microstructural and mechanical evolution of phyllosilicate-bearing fault rock under conditions favouring pressure solution: Journal of Structural Geology, v. 23, no. 8, p. 1187-1202.

Bucher, W. H., 1947, Heart Mountain problem, in Blackstone, D. L., Jr., and Sternberg, C. W., eds., Field Conference Guidebook, field conference in the Bighorn Basin, Wyoming Geological Association, p. 189–197.

Collettini, C., 2011, The mechanical paradox of low-angle normal faults: Current understanding and open questions: Tectonophysics, v. 510, no. 3-4, p. 253-268.

Collettini, C., and Holdsworth, R. E., 2004, Fault zone weakening and character of slip along low-angle normal faults : insights from the Zuccale fault, Elba, Italy: Journal of the Geological Society, v. 161, no. 6, p. 1039-1052.

Collettini, C., and Sibson, R. H., 2001, Normal faults, normal friction?: Geology, v. 29, no. 10, p. 927–930.

Craddock, J. P., Geary, J., and Malone, D. H., 2012, Vertical injectites of detachment carbonate ultracataclasite at White Mountain, Heart Mountain detachment, Wyoming: Geology, v. 40, no. 5, p. 463-466.

Craddock, J. P., Malone, D. H., Magloughlin, J., Cook, A. L., Rieser, M. E., and Doyle, J. R., 2009, Dynamics of the emplacement of the Heart Mountain allochthon at White Mountain: Constraints from calcite twinning strains, anisotropy of magnetic susceptibility, and thermodynamic calculations: Geological Society of America Bulletin, v. 121, no. 5-6, p. 919-938.

Dake, C. L., 1918, The Hart Mountain Overthrust and Associated Structures in Park County, Wyoming The Journal of Geology, v. 26, no. 1, p. 45-55.

Davis, G. A., 1965, Discussion on "Role of fluid pressure in mechanics of overthrust faulting": GSA Bulletin 76:463-474.

Davis, G. H., and Coney, P. J., 1979, Geologic development of Cordilleran metamorphic core complexes: Geology, v. 7, p. 120-124.

Douglas, T. A., Chamberlain, C. P., Poage, M. A., Abruzzese, M., Schultz, S., Henneberry, J., and Layer, P., 2003, Fluid flow and the Heart Mountain fault: a stable isotopic, fluid inclusion, and geochronologic study: Geofluids, v. 3, p. 13-32.

Eiler, J. M., 2007, “Clumped-isotope” geochemistry—The study of naturally-occurring, multiply-substituted isotopologues: Earth and Planetary Science Letters, v. 262, p. 309–327.

Eiler, J. M., 2011, Paleoclimate reconstruction using carbonate clumped isotope thermometry: Quaternary Science Reviews, v. 30, no. 25-26, p. 3575–3588.

Eldridge, G. H., 1894, A geological reconnoissance in northwestern Wyoming: U.S. Geological Survey Bulletin, v. 119.

Engelder, T., 1979, Mechanisms for strain within the Upper Devonian clastic sequence of the Appalachian Plateau, western New York: American Journal of Science, v. 279, no. 5, p. 527-542.

Feeley, T. C., and Cosca, M. A., 2003, Time vs. composition trends of magmatism at Sunlight volcano, Absaroka volcanic province, Wyoming: Geological Society of America Bulletin, v. 115, no. 6, p. 714–728.

Fisher, C. A., 1906, Geology and water resources of the Bighorn Basin, Wyoming: U.S. Geological Survey Professional Paper, v. 53.

Goren, L., Aharonov, E., and Anders, M. H., 2010, The long runout of the Heart Mountain landslide: Heating, pressurization, and carbonate decomposition: Journal of Geophysical Research, v. 115, no. B10.

Gratier, J.-P., Dysthe, D. K., and Renard, F. o., 2013, The role of pressure solution creep in the ductility of the Earth's upper crust: Advances in Geophysics v. 54, p. 47-179.

Gratier, J.-P., Favreau, P., Renard, F., and Pili, E., 2002, Fluid pressure evolution during the earthquake cycle controlled by fluid flow and pressure solution crack sealing: Earth Planets Space, v. 54, p. 1139–1146.

Guo, W. F., Mosenfelder, J. L., Goddard, W. A., III, and Eiler, J. M., 2009, Isotopic fractionations associated with phosphoric acid digestion of carbonate minerals: Insights from first-principles theoretical modeling and clumped isotope measurements: Geochimica et Cosmochimica Acta, v. 73, no. 24, p. 7203–7225.

Han, R., and Hirose, T., 2012, Clay–clast aggregates in fault gouge: An unequivocal indicator of seismic faulting at shallow depths?: Journal of Structural Geology, v. 43, p. 92-99.

Hauge, T. A., 1982, The Heart Mountain detachment fault, northwest Wyoming: involvement of Absaroka volcanic rock: Geology of the Yellowstone Park Area, 33rd Annual Field Conference of the Wyoming Geological Association, p. 175–179.

Hauge, T. A., 1983, Geometry and kinematics of the Heart Mountain detachment fault, northwestern Wyoming and Montana [Ph.D. dissertation]: University of Southern California, 265 p.

Hauge, T. A., 1985, Gravity-Spreading origin of the Heart Mountain allochthon, northwestern Wyoming: Geological Society of America Bulletin, v. 96, p. 1440-1456.

Hauge, T. A., 1990, Kinematic model of a continuous Heart Mountain allochthon: Geological Society of America, v. 102, p. 1174-1188.

Hauge, T. A., 1993a, The Heart Mountain detachment, northwestern Wyoming: 100 years of controversy, in Snoke, A. W., Steidtmann, J. R., and Roberts, S. M., eds., Geology of Wyoming: Geological Survey of Wyoming Memoir 5, p. 530–571.

Hauge, T. A., 1993b, A speedometer for the Heart Mountain allochthon, Wyoming: Geological Society of America Abstracts with Programs, v. 25, no. 5, p. 49.

Hiza, M. M., 2000, The Geochemistry and Geochronology of the Eocene Absaroka Volcanic Province, Northern Wyoming and Southwest Montana, USA [Doctor of Philosophy: Oregon State University, 240 p.

Hubbert, M. K., and Rubey, W. W., 1959, Role of Fluid Pressure in Mechanics of Overthrust Faulting: I. Mechanics of Fluid-Filled Porous Solids and its Application to Overthrust Faulting: Geological Society of America Bulletin, v. 70, p. 115-166.

Hughes, C. J., 1970, The Heart Mountain detachment fault: a volcanic phenomenon?: Journal of Geology, v. 78, no. 107-116.

Huntington, K. W., Eiler, J. M., Affek, H. P., Guo, W., Bonifacie, M., Yeung, L. Y., Thiagarajan, N., Passey, B., Tripati, A., Daeron, M., and Came, R., 2009, Methods and limitations of “clumped” CO2 isotope (Δ47) analysis by gas-source isotope ratio mass spectrometry: Journal of Mass Spectrometry, v. 44, no. 9, p. 1318 –1329.

Lister, G. S., and Davis, G. A., 1989, The origin of metamorphic core complexes and detachment faults formed during Tertiary continental extension in the northern Colorado River region, U.S.A: Journal of Structural Geology, v. 11, p. 65–94.

Melosh, H. J., 1983, Acoustic fluidization: can sound waves explain why dry rock debris appears to flow like a fluid in some energetic geologic events? : American Scientist, v. 71, p. 158-165.

Morley, C. K., 2014, The widespread occurrence of low-angle normal faults in a rift setting: Review of examples from Thailand, and implications for their origin and evolution: Earth-Science Reviews, v. 133, no. 0, p. 18-42.

Nelson, W. H., Prostka, H. J., and Williams, F. E., 1980, Geology and mineral resources of the North Absaroka Wilderness and vicinity, Park County, Wyoming: U.S. Geological Survey Bulletin, v. 1447.

O’Neil, J. R., Clayton, R. N., and Mayeda, T. K., 1969, Oxygen isotope fractionation in divalent metal carbonates: Journal of Chemical Physics, v. 51, p. 5547–5558.

O’Neil, J. R., Clayton, R. N., and Mayeda, T. K., 1969, Oxygen isotope fractionation in divalent metal carbonates: Journal of Chemical Physics, v. 51, p. 5547–5558.

Pierce, W. G., 1957, Heart Mountain and South Fork detachment thrusts of Wyoming: AAPG Bulletin, v. 41, p. 591–626.

Pierce, W.G., 1965a, Geologic map of the Deep Lake quadrangle, Park County, Wyoming: U.S. Geological Survey Quadrangle Map GQ-478, scale: 1:62,500.

Pierce, W.G., 1965b, Geologic map of the Clark quadrangle, Park County, Wyoming: U.S. Geological Survey Quadrangle Map GQ-477, scale: 1:62,500

Pierce, W.G., 1966, Geologic map of the Cody quadrangle, Park County, Wyoming: U.S. Geological Survey Quadrangle Map GQ-542, scale: 1:62,500

Pierce, W.G., 1978, Geologic map of the Cody 1O x 2O Quadrangle, northwestern Wyoming: U.S. Geological Survey Miscellaneous Field Studies Map MF-963, scale: 1:62,500

Pierce, W. G., 1973, Principal features of the Heart Mountain fault, and the mechanism problem, *in* DeJong, K. A., and Scholten, R., eds., Gravity and tectonics.: New York, Wiley, p. 457–471.

Pierce, W. G., 1979, Clastic dikes of the Heart Mountain fault breccia, northwest Wyoming, and their significance: U.S. Geological Survey Professional Paper, v. 1133.

Pierce, W. G., 1980, The Heart Mountain break-away fault, northwestern Wyoming: Geological Society of America Bulletin, v. 91, p. 272-281.

Pierce, W.G., and Nelson, W.H., 1968, Geologic map of the Pat O’Hara Mountain quadrangle, Park County, Wyoming: U.S. Geological Survey Quadrangle Map GQ-755, scale: 1:62,500.

Pierce, W.G., and Nelson, W.H., 1969, Geologic map of the Wapiti quadrangle, Park County, Wyoming: U.S. Geological Survey Quadrangle Map GQ-778, scale: 1:62,500.

Pierce, W.G., and Nelson, W.H., 1971, Geologic map of the Beartooth Butte quadrangle, Park County, Wyoming: U.S. Geological Survey Quadrangle Map GQ-935, scale: 1:62,500.

Pierce, W.G., Nelson, W.H., and Prostka, H.J., 1973, Geologic map of the Pilot Peak quadrangle, Park County, Wyoming and Park County, Montana: U.S. Geological Survey Miscellaneous Investigations Map I-816, scale: 1:62,500.

Pierce, W.G., Nelson, W.H., and Prostka, H.J., 1982, Geologic map of the Dead Indian Peak quadrangle, Park County, Wyoming: U.S. Geological Survey Quadrangle Map GQ-1564, scale: 1:62,500.

Prostka, H.J., Ruppel, E.T., and Christiansen, R.L., 1975, Geologic Map of the Abiathar Peak Quandrangle, Yellowstone National Park, Wyoming and Montana: U.S. Geological Survey Quadrangle Map GQ-1244, scale: 1:62,500.

Rosenbaum, J., and Sheppard, S. M. F., 1986, An isotopic study of siderites, dolomites and ankerites at high temperatures: Geochimica et Cosmochimica Acta, v. 50, no. 6, p. 1147–1150.

Rubey, W. W., and Hubbert, M. K., 1959, Role of Fluid Pressure in Mechanics of Overthrust Faulting: Geological Society of America Bulletin, v. 70, p. 167-206.

Rutter, E. H., 1983, Pressure solution in nature, theory and experiment: Journal of the Geological Society of London, v. 140, no. 5, p. 725-740.

Sales, J. K., 1983, Heart Mountain: blocks in a giant volcanic rock glacier: 34th Annual Field Conference Guidebook of the Wyoming Geological Association, p. 117–165.

Schauble, E. A., Ghosh, P., and Eiler, J. M., 2006, Preferential formation of 13C-18O bonds in carbonate minerals, estimated using first-principles lattice dynamics: Geochimica et Cosmochimica Acta, v. 70, no. 10, p. 2510 –2529.

Smith, S. A. F., Billi, A., Toro, G. D., and Spiess, R., 2011, Principal Slip Zones in Limestone: Microstructural Characterization and Implications for the Seismic Cycle (Tre Monti Fault, Central Apennines, Italy): Pure and Applied Geophysics, v. 168, no. 12, p. 2365-2393.

Swanson, E. M., Wernicke, B. P., Eiler, J. M., and Losh, S., 2012, Temperatures and Fluids on Faults Based on Carbonate Clumped-Isotope Thermometry: American Journal of Science, v. 312, no. 1, p. 1-21.

Swanson, E. M., Wernicke, B. P., and Eiler, J. M., Fluid Flow, Brecciation, and Shear Heating on Faults: Insights from Carbonate Clumped-Isotope Thermometry, submitted to Tectonics

Sylvester, A. G., 1988, Strike-slip faults: Geological Society of America Bulletin, v. 100, p. 1666-1703.

Templeton, A. S., Sweeney, J. J., Manske, H., Tilghman, J. F., Calhoun , S. C., Violich, A., and Chamberlain, C. P., 1995, Fluids and the Heart Mountain fault revisited: Geology, v. 23, no. 10, p. 929-932.

Vasconcelos, C., McKenzie, J. A., Warthmann, R., and Bernasconi, S. M., 2005, Calibration of the δ18O paleothermometer for dolomite precipitated in microbial cultures and natural environments: Geology, v. 33, no. 4, p. 317–320.

Voight, B., 1973, The mechanics of retrogressive block- gliding, with emphasis on the evolution of the Turnagain Heights landslide, Anchorage, Alaska, in DeJong, K. A., and Scholten, R., eds., Gravity and Tectonics: New York, Wiley, p. 97-121.

Wernicke, B., 1995, Low-angle normal faults and seismicity: A review: Journal of Geophysical Research, v. 100, no. B10, p. 20159.

Wernicke, B., Walker, J. D., and Beaufait, M. S., 1985, Structural Discordance between Neogene Detachments and Frontal Sevier Thrusts, Central Mormon Mountains, Southern Nevada: Tectonics, v. 4, no. 2, p. 213-246.

Wright, T. O., and Platt, L. B., 1982, Pressure dissolution and cleavage in the Martinsburg Shale: American Journal of Science, v. 282, no. 2, p. 122-135.

Table 1: Isotopic data of two-toned clastic dike (Fig. 4e) and host rock

Sample ID	δ^{13}C (VPDB)	δ^{18}O-mineral (VSMOW)	Temperature (°C)	δ^{18}O-water (VSMOW)
ES-HM13-41 TA	-0.48	24.98	55.5	-0.56
ES-HM13-41 TB	-0.47	24.96	51.4	-1.24
ES-HM13-41 TC	-0.53	25.01	53.0	-0.93
ES-HM13-41 TD	-0.48	24.59	36.2	4.20
E -HM13-41 TE	-0.55	24.78	42.2	-2.95
ES-HM13-41 TF	-0.56	24.92	41.4	-2.94
Host Bighorn Fm.	1 to -1	23 to 27	50 to 65	-3 to 2

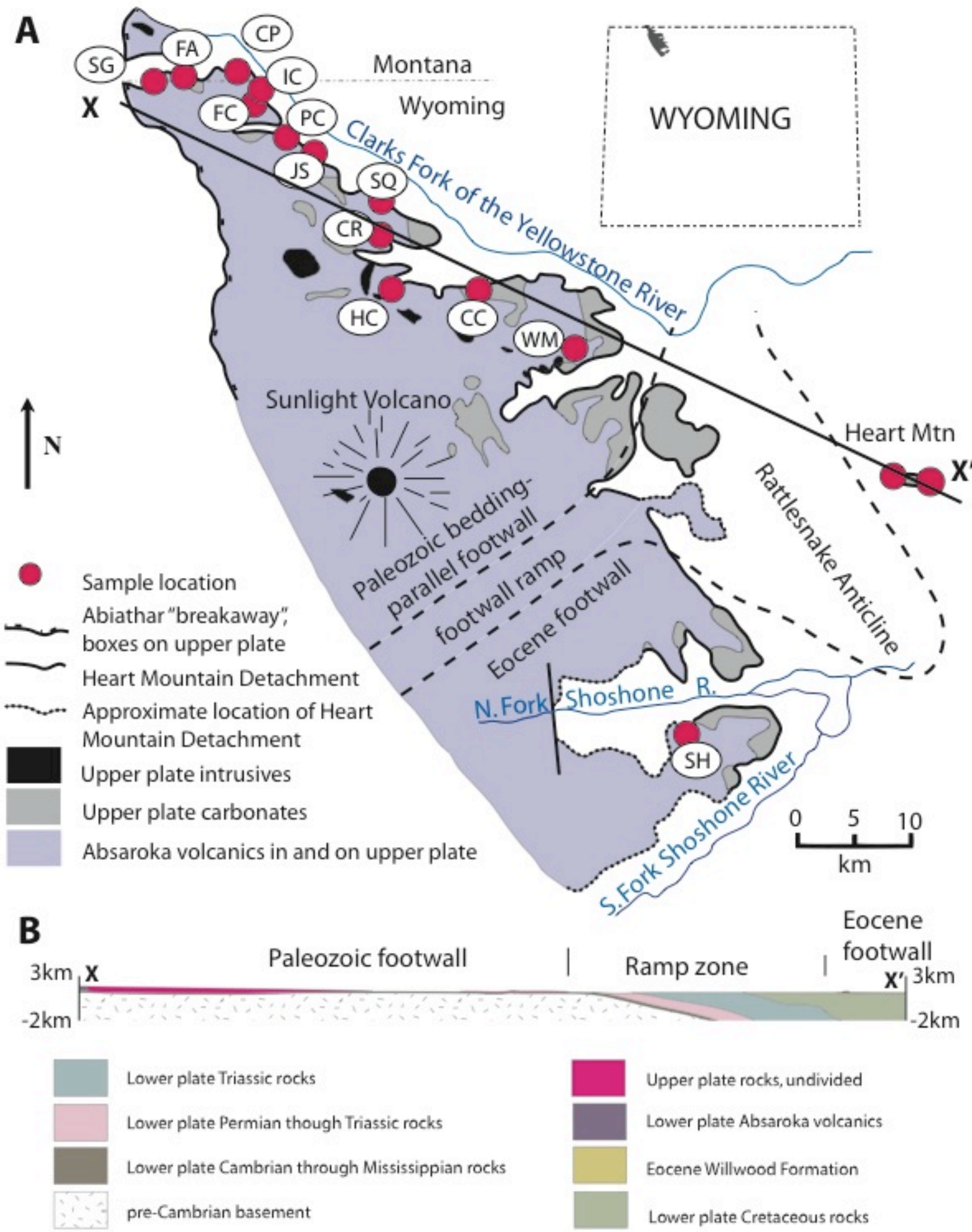

Figure 1. (a) simplified geologic map of the Heart Mountain allochthon showing trace of the basal detachment, distribution of carbonate and volcanic components, footwall sections, location of cross section in (b), and localities discussed in text, from north to south: SG, Silver Gate; FA, Falls Creek; CP, Colter Pass; IC, Index Creek; FC, Fox Creek; PC, Pilot Creek; JS, Jim Smith Creek; SQ, Squaw Creek; CR, Crandall Creek; HC, Hoodoo Creek; CC, Cathedral Cliffs; WM, White Mountain; SH, Sheep Mountain. (b) 1:1 cross section X-X' through Heart Mountain allochthon and substrate.

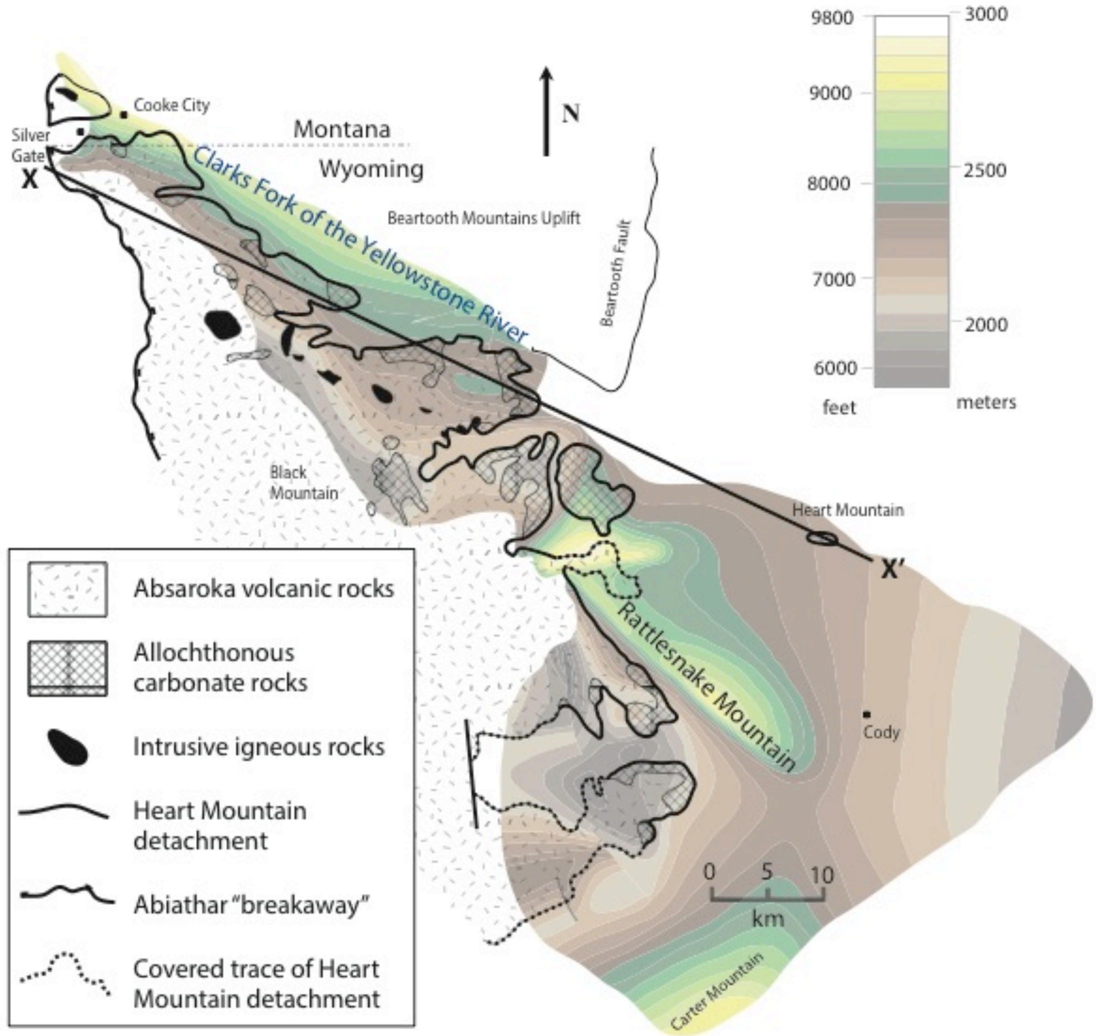

Figure 2. Contour map of the Heart Mountain detachment surface. Line X-X' is the same as shown in Figure 1. Modified from Pierce (1980).

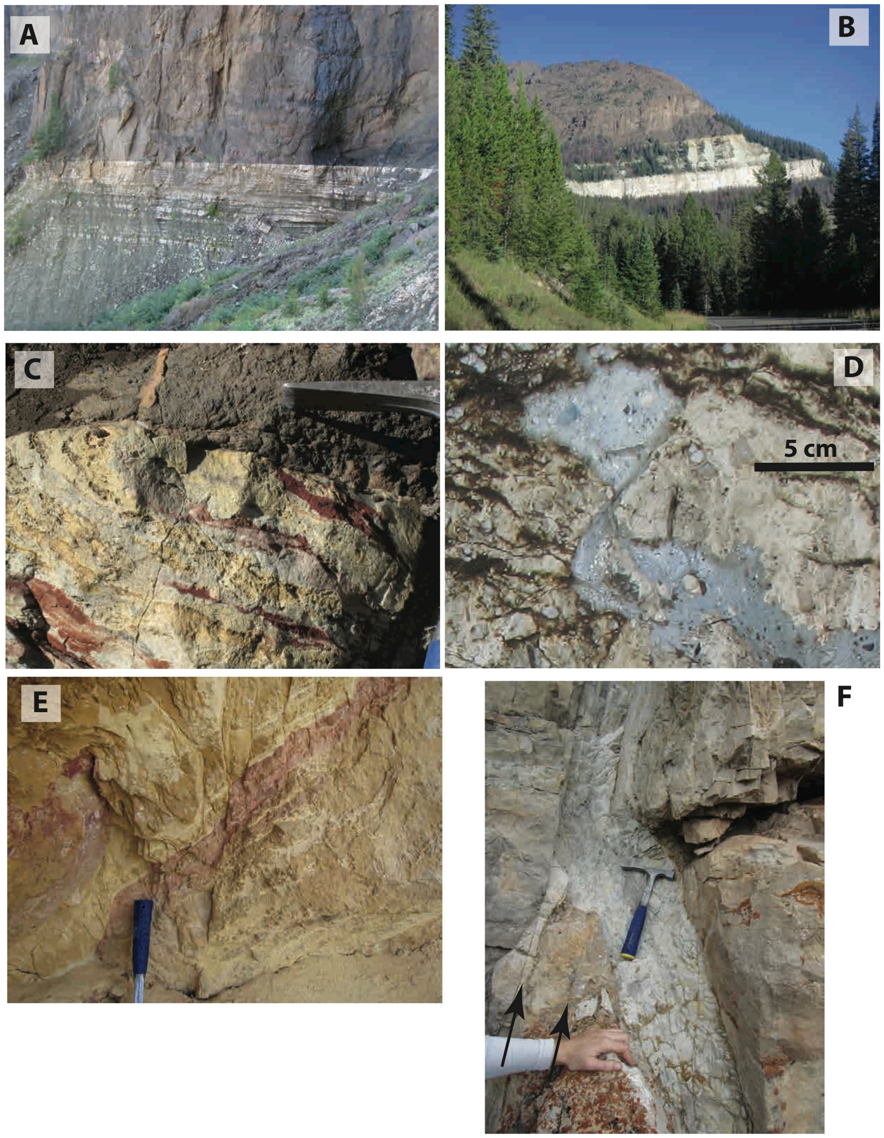

Figure 3. Photographs of megascopic to mesoscopic structural features. (a) Heart Mountain detachment (sharp horizon between dark and light rocks) at Jim Smith Creek (Figure 1), looking south. Dark brown rocks above fault are Absaroka volcanics; massive light-brown cliff below fault is lower 5 m of Bighorn Formation. Light and dark-banded unit below Bighorn Fm. is Cambrian Snowy Range Fm. (b) Heart Mountain detachment (sharp contact between dark and light rocks) above Index Creek; light colored cliffs c. 200 m high. (c) Heart Mountain detachment (base of dark brown unit), showing brecciated and mineralized layering in Bighorn Fm. in footwall truncated by fault; light-brown, cm-scale clastic dike visible upper left; Jim Smith Creek, looking SW; hammer for scale. (d) Clastic dike intruding lineated cataclasite, subsequently drag-folded and offset by mesoscale fault, Fox Creek. (e) offsets of hematitic foliated gouge within hanging wall fault zone, Heart Mountain; hammer for scale. (f) clastic dike (beneath hammer) deformed by flexure and jigsaw brecciation in association with small hanging wall faults (black arrows), Crandall Creek.

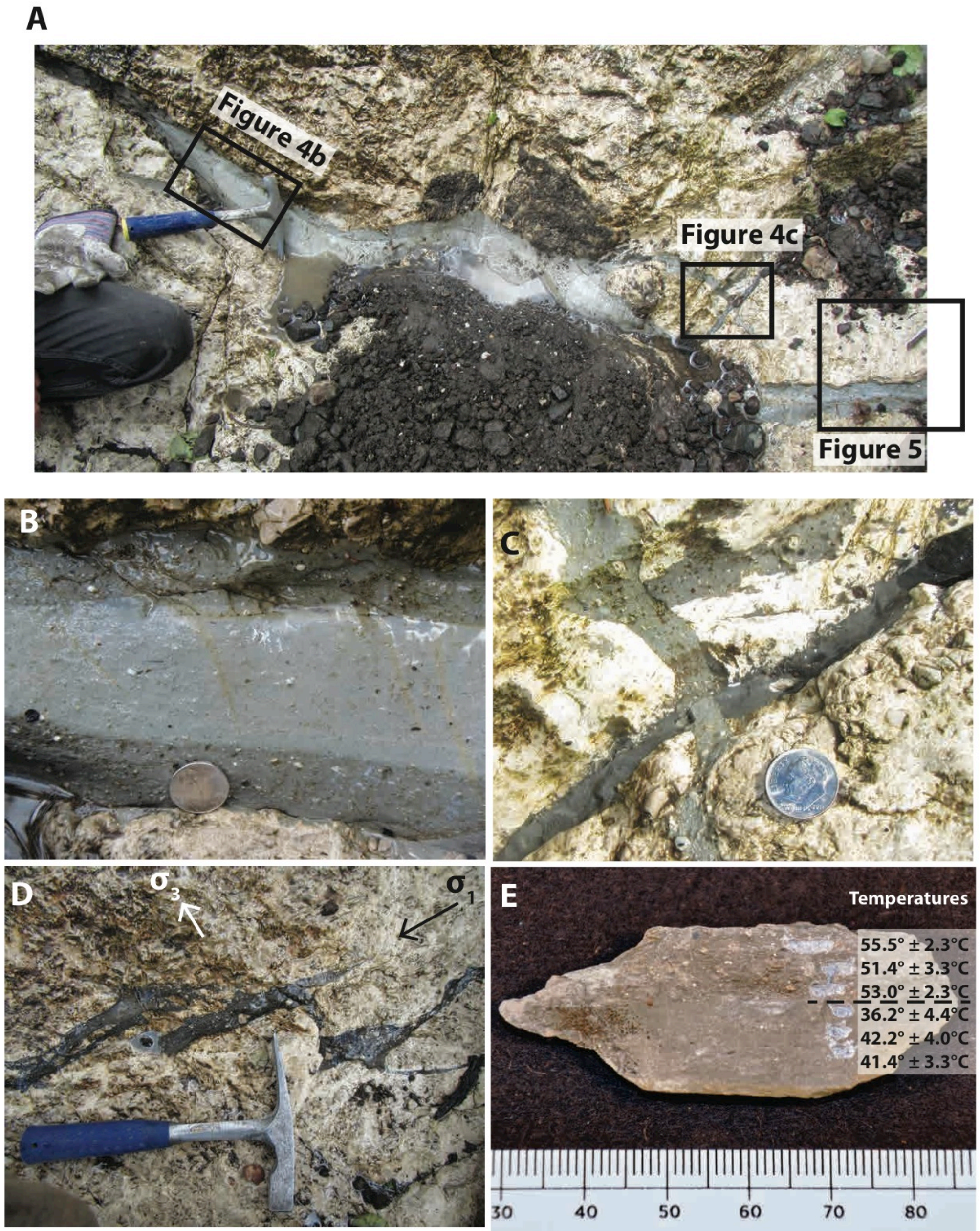

Figure 4: Photographs of clastic dikes at Fox Creek c. 5-10 m above Heart Mountain detachment. (a) Overview looking SW and downward at 45° angle; black outlines show locations of (b), (c) and Figure 5; hammer is 28 cm long. (b) Closeup of two-toned clastic dike; coin is 21 mm in diameter. (c) Cross-cutting clastic dikes, with older light and dark gray phases, inclined to the left, being truncated at high angle by a younger light gray clastic dike; coin is 18 mm in diameter. (d) View W of en-echelon clastic dikes, with hammer handle oriented parallel to detachment. Arrows indicate implied maximum (σ_1, black) and minimum (σ_3, white) principal stress orientations. (e) Hand sample of main two-toned clastic dike shown in (b), showing microdrill pits and corresponding carbonate clumped-isotope temperatures; black dashed line marks the boundary between the darker phase (upper) and lighter phase (lower) of the dike; scale in mm.

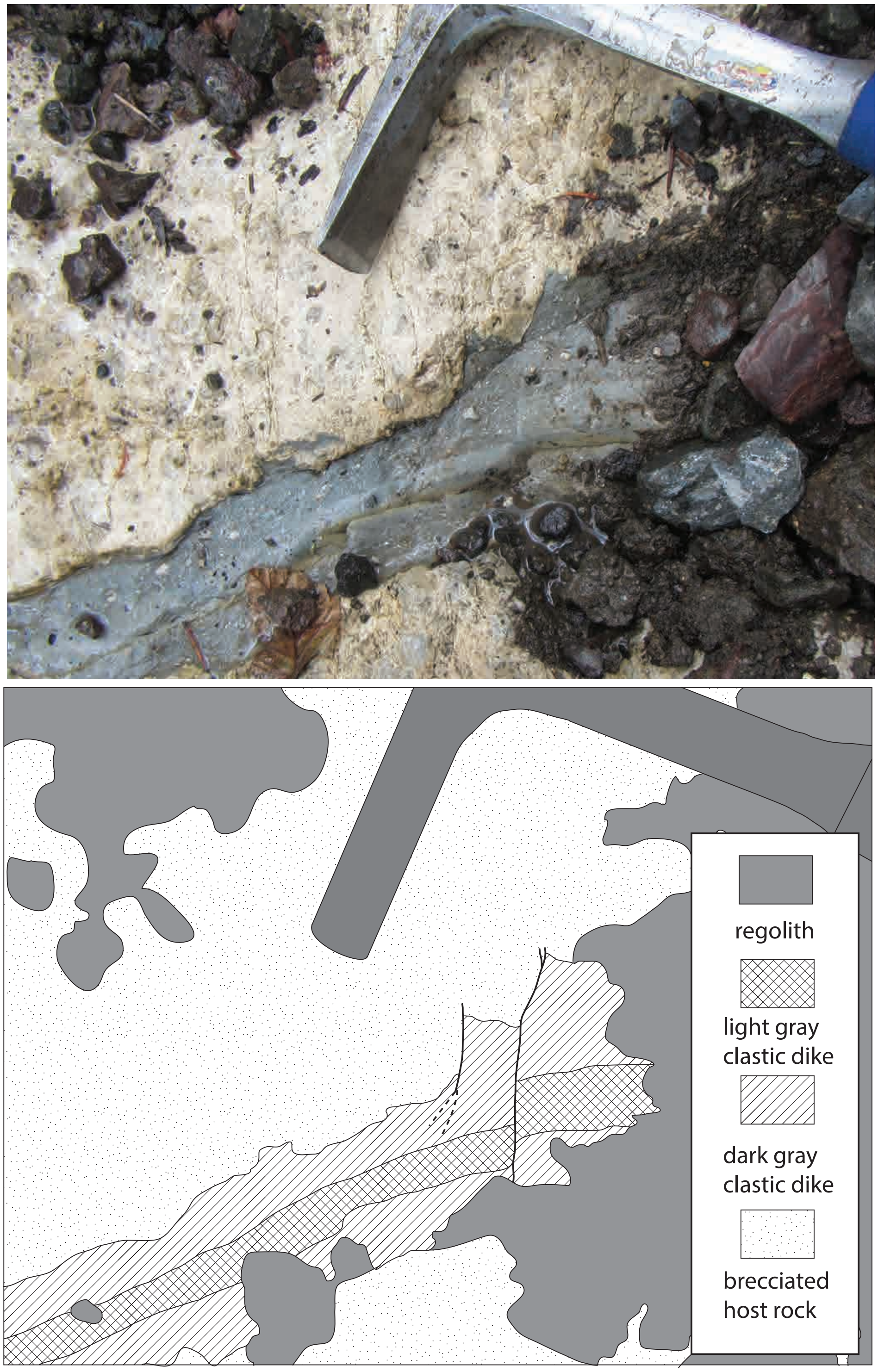

Figure 5: Photograph and interpretive line drawing of a clastic dike, suggesting five discrete episodes of injection and deformation: 1, brecciation of the host rock; 2, injection of the dark gray (diagonal ruled) clastic dike; 3, offset along the left fault; 4, injection of the light gray (cross-hatched) clastic dike; and 5, offset of both clastic dikes along the right fault.

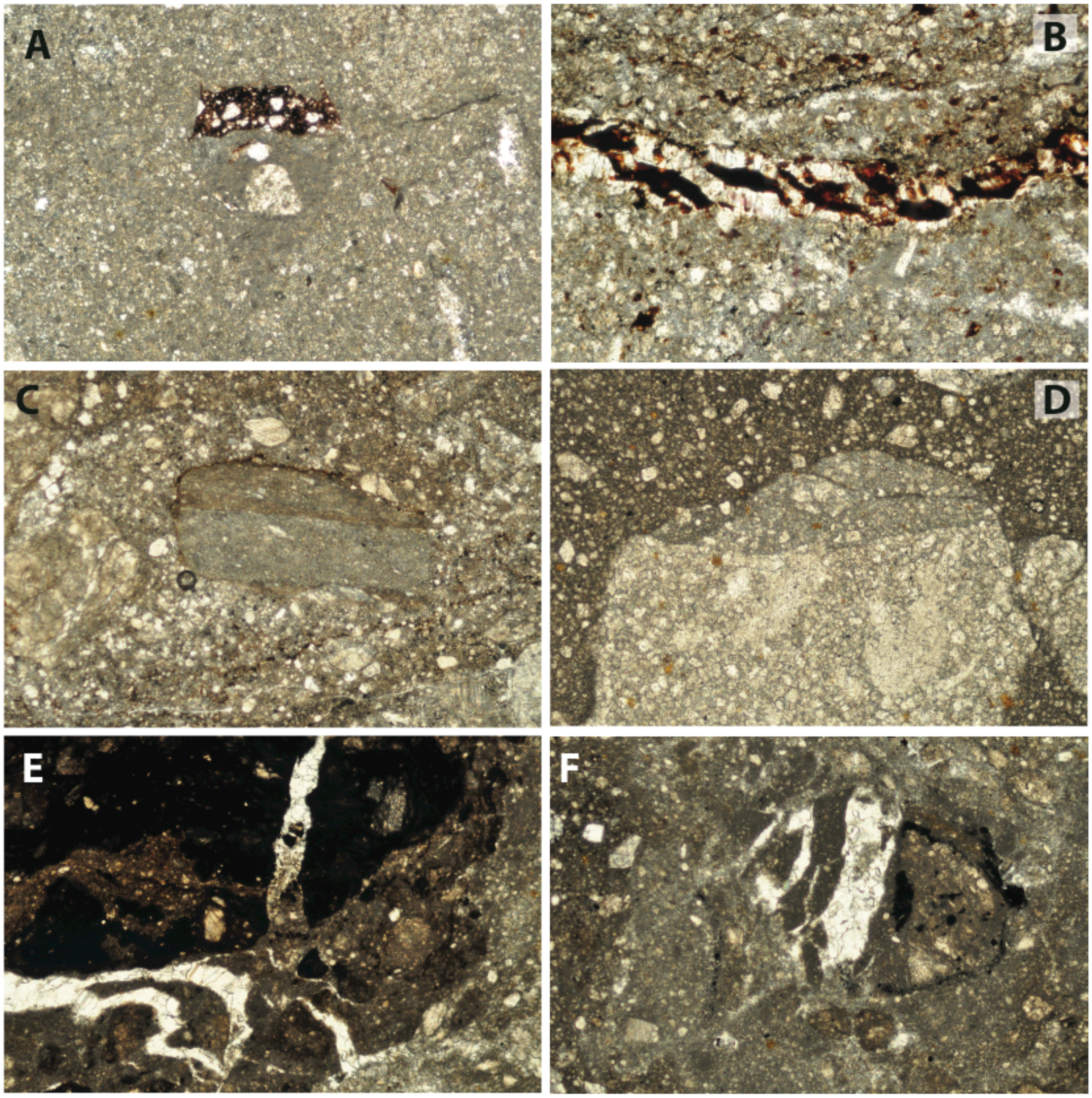

Figure 6: Photomicrographs showing multiple episodes of brecciation. All images have 2.2 mm-wide field of view. (a) Rounded clast in center contains previous volcanic breccia (dark material at top) adjacent to carbonate breccia, hanging wall, White Mountain; (b) Vein showing sheeted texture suggestive of progressive in-filling with calcite and Fe oxides during deformation, hanging wall, Squaw Creek; (c) Clast of older fine-grained breccia with a rim of insoluble residues, surrounded by coarser-grained, younger breccia, footwall at Jim Smith Creek; (d) Clast with three discrete brecciation events, each with different proportion of clasts, footwall at Jim Smith Creek; (e) Clast showing progressive brecciation and calcite veining, footwall, Jim Smith Creek; (f), Clast preserving veining event between two episodes of brecciation.

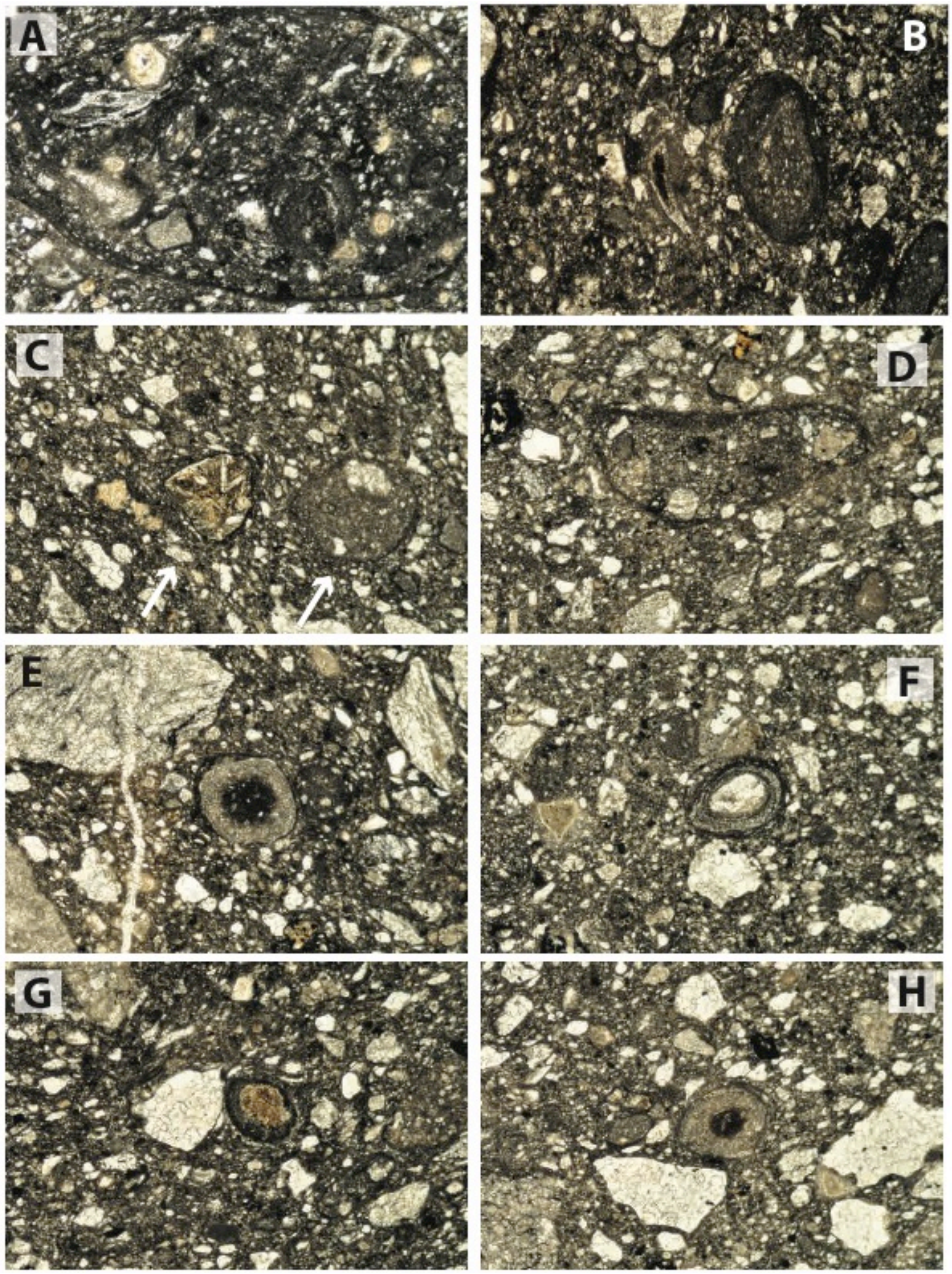

Figure 7: Photomicrographs of 12 banded grains from a single thin section from White Mountain (sample ES-HM12-06). All photos had field of view of 1.5 x 2.2 mm. They vary in form, and also in the degree to which they visibly contrast with the host breccia. Some are defined by reaction rims, some are bounded by dark seams that are not always spherical, and many have dissolution seams in the matrix outside the grains, parallel to the grain boundary.

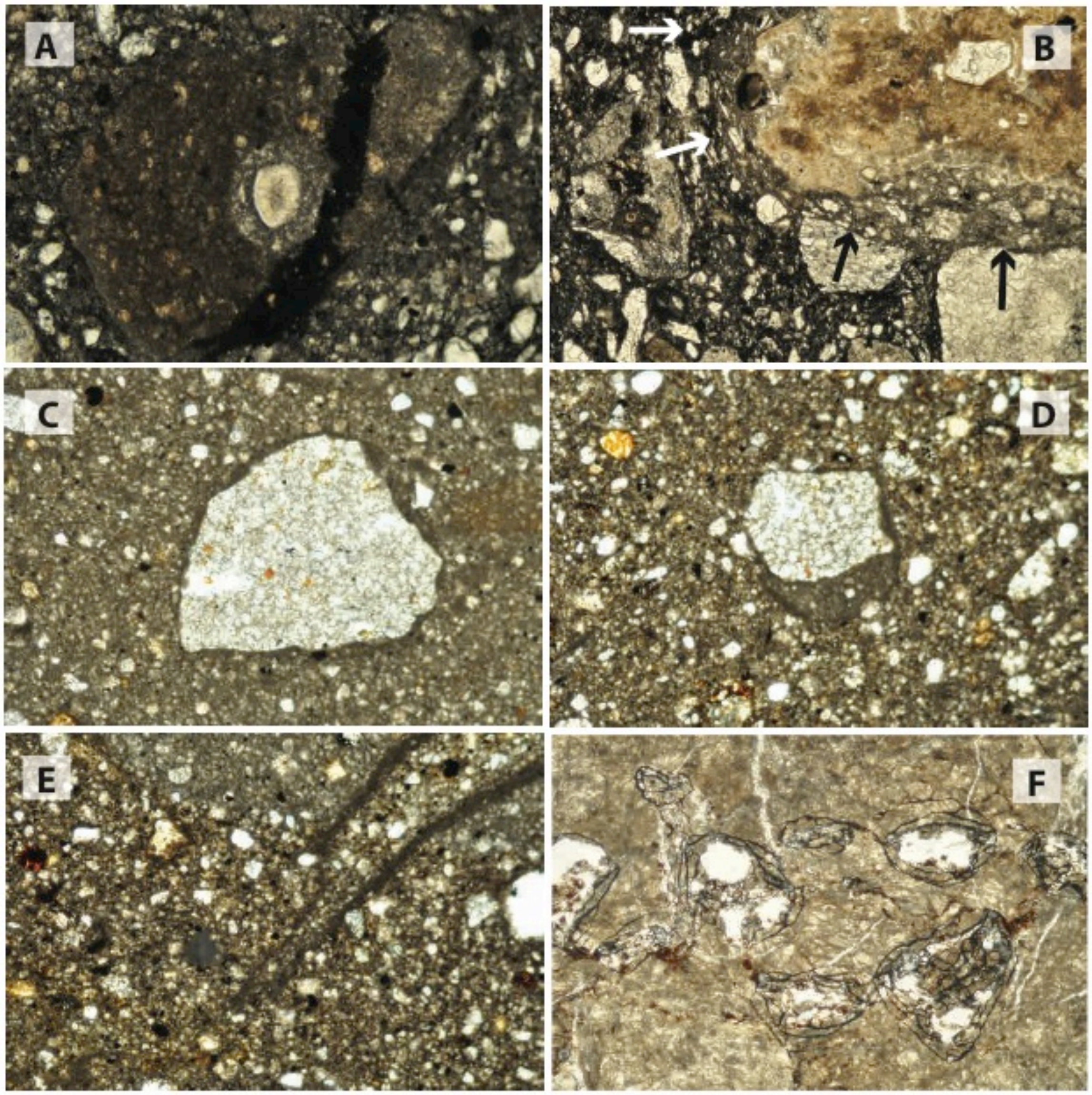

Figure 8. Photomicrographs showing textures similar to those found in banded grains. (a) and (b), detachment plane breccia, White Mountain; (c), (d) and (e), clastic dike near Crandall Creek; (f) detachment plane breccia, Mormon Peak detachment, southern Nevada. Field of view is 2.2 mm wide, except in (a) where it is 0.9 mm wide. (a), Light-colored zone of alteration overprinting older dark layer, which truncates breccia texture from an earlier event; (b), a "brown clast" (upper right) with concentric bands of dissolution seams; arrows show trace of dissolution seam that truncates a rounded carbonate grain in exterior breccia; smaller grains (~100 microns) have preferred orientation tangential to core grain; (c), rounded carbonate clast with an alteration (?) rim filling in concavities at edge; (d), rounded carbonate clast with an alteration rim similar to, but large than, that found in (c); (e), quasi-planar dissolution seams like those found in banded grains; (f), sample

exhibiting round pressure solution seams associated with stylolitization, a potential precursor to banded grains at Heart Mountain.

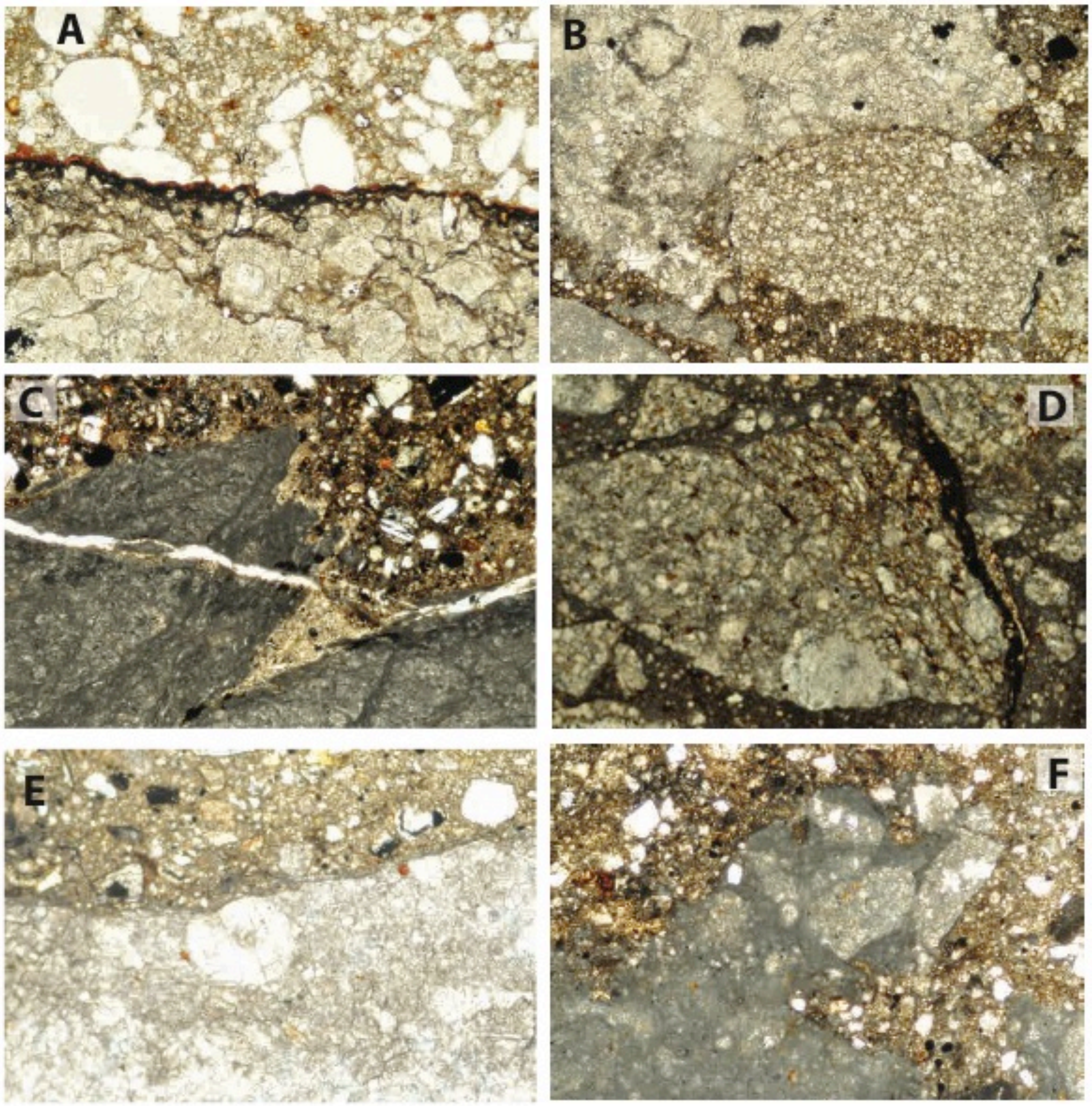

Figure 9. Photomicrographs showing different styles of pressure solution. All images are 2.2 mm across. (a), stylolite from near Index Peak with thick seam of iron oxide and insoluble residues; (b), pressure solution, with smaller, rounded grain with fine-grained texture penetrating larger, more angular grain with coarser texture, from footwall at Jim Smith Creek; (c), pressure solution and veining along highly irregular contact between carbonate (dark gray) and volcanic (brown) phases of breccia, NW side of Sheep Mountain; (d), breccia clast within breccia containing stylolites, indicating dissolution between two fragmentation-cementation events, from north of Pilot Creek. (e), irregular, stylolitic contact along Heart Mountain detachment surface at Hoodoo Creek; (f) highly irregular stylolitic contact between volcanic breccia and carbonate breccia at the detachment, south of Pilot Creek.

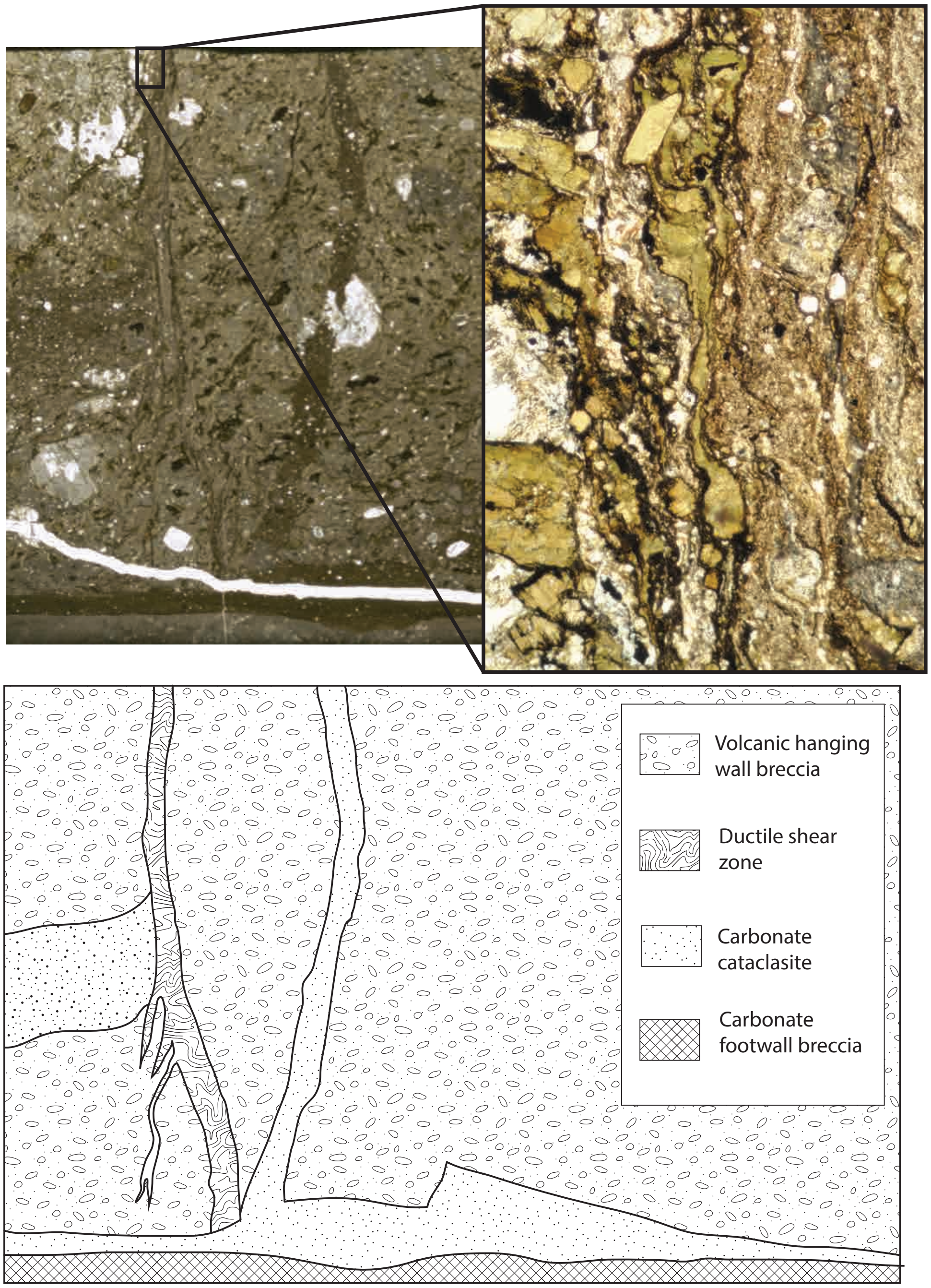

Figure 10. Photomicrograph of the Heart Mountain detachment at Jim Smith Creek, and interpretive sketch of textures; inset photo has height of 2.2 mm. A zone of ductile deformation offsets a clastic dike filled with carbonate breccia, but is offset by the carbonate cataclasite layer on the detachment surface. Inset photo shows detail of shear zone, including sigmoidal clasts of hornblende and carbonate grains.

A

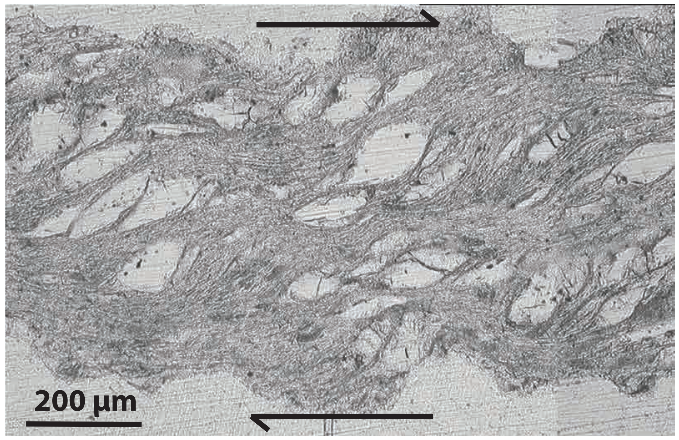

B

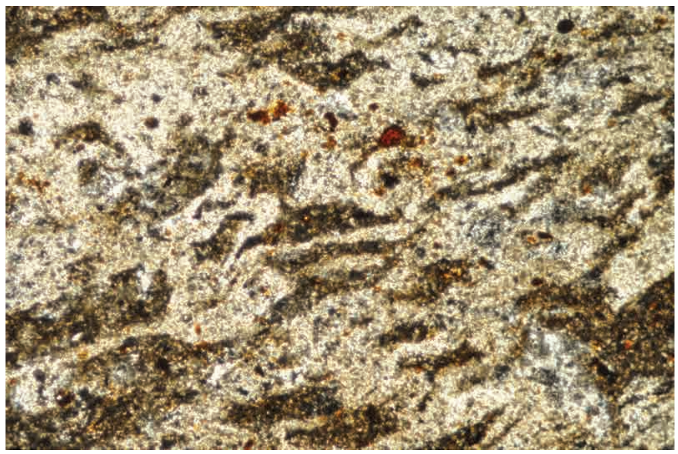

C

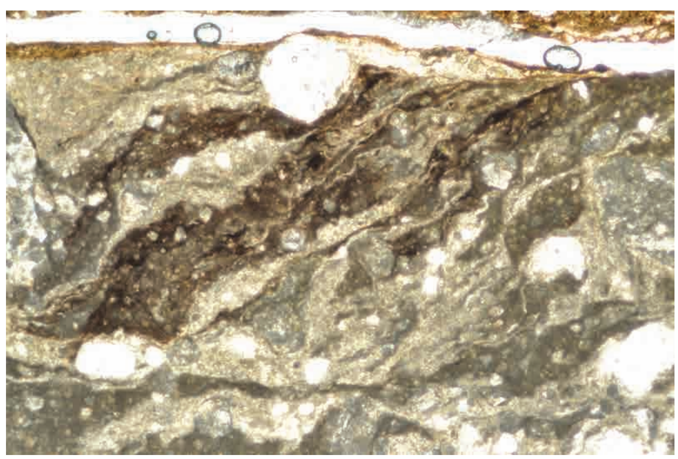

Figure 11. Photomicrographs, sigmoid-shaped grains, (a) generated by high-strain brittle-viscous creep via pressure solution, using halite-kaolinite aggregates (from Bos and Spiers, 2001, their figure 5c); (b) deformed basal Bighorn Formation from just below the detachment, Pilot Creek; sigmoidal carbonate pods resemble features in (a) associated with viscous creep; (c) footwall just below the Heart Mountain detachment (subhorizontal breccia zone in uppermost left corner), showing brittle shear and the formation of sigmoidal banding similar to the experimental texture in (a). Width of view in (b) and (c) is 2.2 mm, and long axis is parallel to the detachment in (b) and (c).

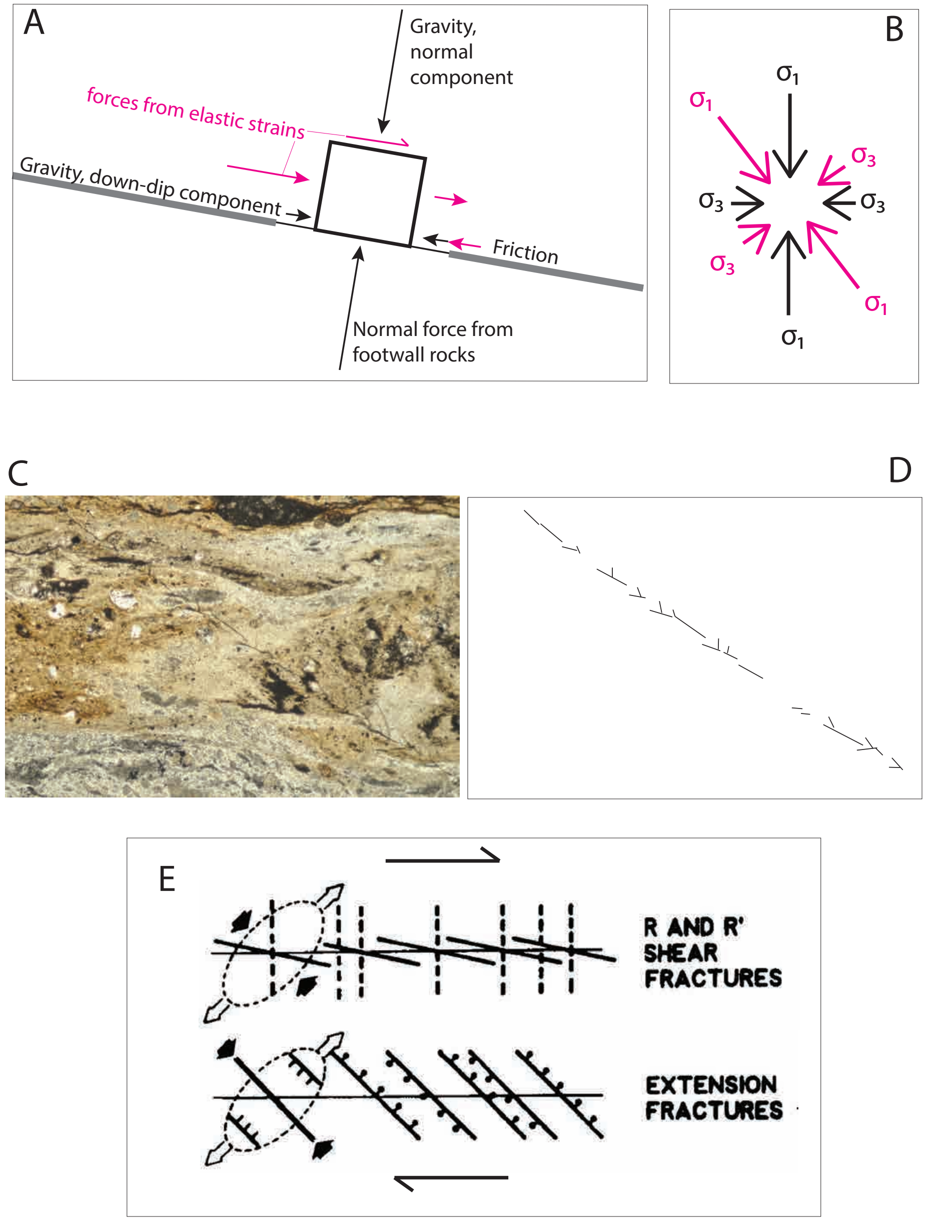

Figure 12: diagrams showing rotation of principal stress axes due to elastic forces. (a) schematic block diagram showing the forces on an arbitrary piece of rock on a low-angle fault, here dipping 10°, with creeping sections (thick gray lines) and a non-creeping section (thin black line). Forces from gravity and friction shown with black arrows and those that would result from the elastic strain in neighboring rocks shown in red arrows; (b) principal stress orientations predicted from just gravity and friction (black) and from the inclusion of elastic forces (red); (c), detachment gouge from Jim Smith Creek overprinted with Riedel shear fractures; (d), drawing highlighting the orientations of fractures in C; (e), diagram from Sylvester, 1988 showing the orientations of Riedel and tensional fractures predicted from the given maximum principal compression direction (black arrows) and the least compressive direction (white arrows).